Novel non-equilibrium critical behavior in unidirectionally coupled stochastic processes

Yadin Y. Goldschmidt[1], Haye Hinrichsen[2], Martin Howard[3,*], and Uwe C. Täuber[4,*]
[1] *Department of Physics and Astronomy, University of Pittsburgh, Pittsburgh PA 15260, U.S.A.*
[2] *Max-Planck-Institut für Physik komplexer Systeme, Nöthnitzer Straße 38, D-01187 Dresden, Germany*
[3] *CATS, The Niels Bohr Institute, Blegdamsvej 17, 2100 Copenhagen Ø, Denmark*
[4] *Institut für Theoretische Physik, Technische Universität München, James-Franck-Straße, D-85747 Garching, Germany*
(July 13, 2011)

Phase transitions from an active into an absorbing, inactive state are generically described by the critical exponents of directed percolation (DP), with upper critical dimension $d_c = 4$. In the framework of single-species reaction-diffusion systems, this universality class is realized by the combined processes $A \to A+A$, $A+A \to A$, and $A \to \emptyset$. We study a hierarchy of such DP processes for particle species $A, B, \ldots$, *unidirectionally* coupled via the reactions $A \to B, \ldots$ (with rates $\mu_{AB}, \ldots$). When the DP critical points at all levels coincide, *multicritical* behavior emerges, with density exponents β_i which are markedly reduced at each hierarchy level $i \geq 2$. This scenario can be understood on the basis of the mean-field rate equations, which yield $\beta_i = 1/2^{i-1}$ at the multicritical point. Using field-theoretic renormalization group techniques in $d = 4-\epsilon$ dimensions, we identify a new crossover exponent ϕ, and compute $\phi = 1 + O(\epsilon^2)$ in the multicritical regime (for small μ_{AB}) of the second hierarchy level. In the active phase, we calculate the fluctuation correction to the density exponent on the second hierarchy level, $\beta_2 = 1/2 - \epsilon/8 + O(\epsilon^2)$. Outside the multicritial region, we discuss the crossover to ordinary DP behavior, with the density exponent $\beta_1 = 1 - \epsilon/6 + O(\epsilon^2)$. Monte Carlo simulations are then employed to confirm the crossover scenario, and to determine the values for the new scaling exponents in dimensions $d \leq 3$, including the critical initial slip exponent. Our theory is connected to specific classes of growth processes and to certain cellular automata, and the above ideas are also applied to unidirectionally coupled pair annihilation processes. We also discuss some technical as well as conceptual problems of the loop expansion, and suggest some possible interpretations of these difficulties.

PACS numbers: 64.60.Ak, 05.40.+j, 82.20.-w.

I. INTRODUCTION

The notion of *universality* plays a central role in equilibrium as well as in non-equilibrium statistical mechanics. It was first used by experimental physicists in order to describe the observation that certain thermodynamic observables measured in different and apparently unrelated equilibrium systems near a continuous phase transition may exhibit the same type of singular behavior [1]. It was, in fact, then realized that the majority of equilibrium critical phenomena belong to very few *universality classes* which are characterized by a certain set of critical exponents. In order to explain universality, various theoretical approaches have been constructed, for example scale invariance [2], field-theoretic renormalization group techniques [3], and the theory of conformal invariance [4], which predicts a series of universality classes for two-dimensional critical systems. Thus in equilibrium statistical mechanics, especially in two dimensions, the concept of universality seems to be well understood.

For systems far from equilibrium, however, the situation near dynamic continuous phase transitions is less clear. Non-equilibrium processes are much harder to solve or even to characterize exactly since the probability distribution cannot be obtained from an energy functional, but has to be derived directly from the equations of motion. In addition, systems far from equilibrium are in general not conformally invariant since there is no symmetry between spatial and temporal degrees of freedom. Nevertheless it appears that universality, although probably in a weaker sense, may also play an important role in non-equilibrium critical phenomena. As in the case of equilibrium physics the picture that emerges is that only a few distinct universality classes seem to exist. The known examples include phase transitions in driven diffusive systems [5], the power-law decay in annihilation-coagulation processes [6–8], the "parity-conserving" dynamic transition for branching and annihilating random walks with even offspring number [9], non-equilibrium roughening transitions in growth models [10], specifically in the KPZ equation [11], and the critical points of directed percolation [12], as described by Reggeon field theory [13], and of dynamic (isotropic) percolation [14]. As a unifying theoretical framework is not yet available, we are still far from a systematic classification of non-equilibrium critical phenomena. Therefore one important direction of research is in fact to search for further unknown universality classes.

Another direction, which is actually the objective of the present paper, would be to investigate the known universality classes in more complicated contexts. The basic idea is to use several non-equilibrium systems of a known universality class as building blocks of a superior structure in which the systems are linked to each other in

a specific manner. The question posed is whether these systems can be combined in such a way that novel critical behavior emerges. In other words, is it possible to couple several non-equilibrium systems of a given universality class in such a manner that the resulting critical behavior is characterized by independent critical exponents?

Such a model with *quadratically* coupled directed percolation (DP) processes was recently investigated by Janssen, who found that despite the apparent complexity of this coupled multi-species system, the universality class of the active / absorbing transition was that of DP itself [15]. In the present article we show that novel critical behavior may, however, occur when several copies of the same non-equilibrium process are *linearly* coupled in one direction without feedback. More precisely, we consider a linear hierarchy of *unidirectionally* coupled copies A,B,C,... of the *same* non-equilibrium system:

$$A \to B \to C \to \dots \tag{1.1}$$

The systems are coupled in such a way that the dynamical processes at a certain level in the hierarchy depend on the state at the preceding level but not vice versa. For example, subsystem A, the lowest level in the hierarchy, is not influenced by the dynamics of B and C and thus it evolves independently as if the other hierarchy levels did not exist. Subsystem B in turn is affected by A but not by C, and hence this is the first level in the hierarchy where novel critical behavior might occur. The hierarchy can be continued to infinitely many levels. However, because of the unidirectional structure one can always truncate the hierarchy at some level without affecting the temporal evolution at lower levels. For example, we may consider a two-level hierarchy $A \to B$ or a three-level hierarchy $A \to B \to C$; in both cases the dynamics of the subsystems A and B would be exactly the same.

The most interesting behavior of the composite system is expected when the subsystems $A, B, C, \dots$ themselves are close to criticality. This usually happens when the isolated subsystems would undergo a continuous non-equilibrium phase transition. Let us assume that the stochastic process under consideration is controlled by a single parameter p with a phase transition taking place at $p = p_c$. A unidirectionally coupled hierarchy of such processes is thus controlled by a sequence of independent control parameters $p^{(A)}, p^{(B)}, p^{(C)}, \dots$, which means that the composite system is described by a high-dimensional phase diagram. When all levels are critical (i.e. $p^{(A)} = p^{(B)} = p^{(C)} = \dots = p_c$), a complex interplay of long-range correlations is expected. We will refer to this special point in the phase diagram as a *multicritical point*. In the vicinity of this point the properties of the entire system depend crucially on the direction from which it is approached, resulting in interesting *multicritical behavior*. In particular we will consider the special case $p^{(A)} = p^{(B)} = p^{(C)} = \dots = p$, where the entire hierarchy is controlled by a single parameter.

The outlined concept of unidirectionally coupled non-equilibrium processes is quite general and may be applied to various dynamical systems. But, as we shall also see, this mechanism does not necessarily lead to new universality classes in all cases, and we have already mentioned the quadratically coupled DP processes [15] as one counterexample. In the present work we will focus on non-equilibrium processes which display a continuous phase transition from a fluctuating into an absorbing state, i.e. a configuration which once reached, cannot be escaped from.

The canonical example for a transition into an absorbing state is the critical point of directed percolation (DP). In DP, sites of a lattice are either occupied by a particle (active) or empty (inactive). The dynamic processes are that a particle can self-destruct or produce an offspring at a neighboring empty site. If the rate for offspring production p is very low, the system always reaches a state without particles which is the absorbing state of the system. On the other hand, when p exceeds a certain critical value p_c, another steady state with a finite particle density exists on the infinite lattice. In between a continuous phase transition takes place which is characterized by long-range power-law correlations. Another example considered in the present work is the annihilation process $A + A \to 0$ [7,8] in which the particle density decays as $t^{-d/2}$ in dimensions $d < 2$. Here the absorbing state (the empty lattice) is approached without the tuning of any parameter, i.e. the process is "critical" by itself.

To construct a unidirectionally coupled hierarchy of such processes we implement additional dynamical rules which allow each particle at a given level in the hierarchy to induce the creation of a new particle at the same lattice site of the next level. This ensures that the composite system still has an absorbing state, namely the empty state without particles. More precisely, a whole hierarchy of absorbing subspaces is generated. For example, if subsystem A enters the inactive state, it will never become active again and therefore the dynamical processes are restricted to an absorbing subspace where only $B, C, \dots$ may fluctuate. This subspace in turn contains another absorbing subspace in which B is inactive, etc. As we will demonstrate, such a hierarchy of systems with absorbing states coupled by induced particle creation is characterized by a subset of novel critical exponents. It should be emphasized that the emergence of novel critical behavior is related to the fact that the processes are coupled in only one direction. Even a very small feedback (e.g. $B \to A, C \to B$) or cyclic closure (e.g. $A \to B \to C \to A$) would destroy this new feature.

In this article we present a detailed analysis of unidirectionally coupled DP [16]. For the case of equal control parameters it is observed that the asymptotic particle densities near the multicritical point are characterized by different critical exponents $\beta_A, \beta_B, \beta_C, \dots$. Since level A evolves independently, β_A is just the usual density exponent of DP. At higher levels numerical estimates show that the density exponents are considerably reduced compared to their DP values. In Sec. II we discuss the mean-field theory of coupled DP which already explains why the density exponents at higher levels are reduced. It also allows us to study crossover phenomena close to

the multicritical point. Mean-field theory is expected to hold above the DP critical spatial dimension $d_c = 4$. For $d < d_c$ the numerically observed values for the density exponents are much smaller, which means that the mean-field results are strongly modified by fluctuation effects. In order to understand these reduced values, we recently derived the critical exponents to one-loop order [16] by means of a field-theoretical renormalization group analysis, based on the "Hamiltonian" representation of the classical master equation [8,17,18]. In Sec. III we present these calculations in detail, including a discussion of the diagonalized and multicritical theories, respectively, the active phase, logarithmic corrections at $d_c = 4$, crossover studies, and the critical behavior at higher levels in the hierarchy. The field-theoretical results are supported by extensive numerical simulations in Sec. IV, while in Sec. V various applications of coupled DP are demonstrated. The examples of coupled annihilation and other closely related topics are the subjects of Sec. VI. Finally, a critical discussion of some technical as well as conceptual problems arising in the field-theoretic approach are the subject of our conclusions in Sec. VII.

II. COUPLED DP PROCESSES: MEAN-FIELD APPROXIMATION

In the bulk of this paper, we shall study unidirectionally coupled directed-percolation processes. It is convenient to represent these processes in the framework of reaction-diffusion systems. The starting point of the hierarchy of coupled systems is therefore the following reaction scheme, which can be viewed as the prototype for the active / absorbing state transitions in the directed-percolation universality class [13]:

$$A \to A + A \quad \text{with rate } \sigma_A \ , \tag{2.1}$$

$$A \to \emptyset \quad \text{with rate } \mu_A \ , \tag{2.2}$$

$$A + A \to A \quad \text{with rate } \lambda_A \ . \tag{2.3}$$

We can immediately write down the corresponding rate equations for the particle density $n_A(t)$; this description neglects fluctuation and correlation effects, and therefore corresponds to a mean-field approximation. The average particle number is increased via the branching reaction (2.1), and reduced via both the decay (2.2) and coagulation (2.3). However, while the first two processes occur spontaneously, with rates σ_A and μ_A, respectively, and therefore the change in particle number is proportional to the particle density itself, the coagulation reaction requires that two particles A meet on the same lattice site (in a discrete representation), and hence the total particle loss due to the process (2.3) is proportional to the density squared. This yields the balance equation

$$\frac{\partial n_A(t)}{\partial t} = (\sigma_A - \mu_A) n_A(t) - \lambda_A n_A(t)^2 \ . \tag{2.4}$$

As we are considering local reactions only, we may generalize this mean-field equation slightly by considering a coarse-grained local particle density $n_A(x,t)$, and supplementing Eq. (2.4) with a diffusion term,

$$\frac{\partial n_A(x,t)}{\partial t} = D \left(\nabla^2 - r_A \right) n_A(x,t) - \lambda_A n_A(x,t)^2 \ . \tag{2.5}$$

Here we have introduced the diffusion constant D, and defined $r_A = (\mu_A - \sigma_A)/D$.

Obviously, the mean-field dynamic phase transition occurs at the point $r_A = 0$, where the balance of gain and loss due to the processes linear in n_A changes sign. For $r_A > 0$, the only stationary state of Eq. (2.5) is $n_A = 0$, and for $t \to \infty$ the particle density will simply decay to zero according to $n_A(t) \to e^{-D r_A t}$, because once the particle density has become sufficiently small, the coagulation contribution can be neglected. Furthermore, $n_A = 0$ represents an absorbing phase, because once there are no particles left in the system, none of the processes (2.1)–(2.3) can happen any longer — hence all fluctuations cease, and the system cannot escape from this state. For $r_A < 0$, on the other hand, there is another stationary state with non-zero particle density

$$n_A = D|r_A|/\lambda_A \ , \tag{2.6}$$

which can be viewed as the order parameter of the active phase. In the active state, the asymptotic density is approached exponentially again, with the characteristic rate $D|r_A|$. Precisely at the transition, only the term proportional to n_A^2 survives in Eq. (2.5), which therefore becomes identical to the mean-field rate equation for diffusion-limited coagulation or annihilation [6]. The solution to Eq. (2.4) then becomes

$$n_A(t) \sim 1/t \ , \tag{2.7}$$

i.e., the density decays according to a power law at the critical point.

Upon identifying $r_A = p_c - p$, where p_c denotes the percolation threshold, we can translate the above mean-field results to the notation of directed percolation. Eq. (2.5) implies that the characteristic length scale $\xi_\perp = |r_A|^{-1/2}$ diverges in the vicinity of the transition,

$$\xi_\perp \sim |r_A|^{-\nu_\perp} \ , \quad \nu_\perp = 1/2 \ . \tag{2.8}$$

At the critical point, the exponential decay rates vanish, and the characteristic frequency becomes diffusive, $\omega_c \sim D q^2$; hence

$$\omega_c \sim q^z \ , \quad z = 2 \ . \tag{2.9}$$

Equivalently, upon approaching the critical point, the characteristic time scale diverges according to

$$\xi_\parallel \sim |r_A|^{-\nu_\parallel} \ , \quad \nu_\parallel \equiv z \nu_\perp = 1 \ . \tag{2.10}$$

Also, at $p = p_c$,

$$n_A(t) \sim t^{-\alpha} \ , \quad \alpha = 1 \ . \tag{2.11}$$

Finally, in the active phase near the transition, the order parameter grows as

$$n_A \sim |r_A|^\beta \ , \quad \beta = 1 \ . \tag{2.12}$$

Notice that the exponents α and β are related, provided the following scaling relation holds,

$$n_A(r_A, x, t) = |r_A|^\beta \hat{n}_A(x/\xi_\perp, t/\xi_\parallel) \ . \tag{2.13}$$

For then at $p = p_c$, $\hat{n}_A(0, y) \sim y^{-\beta/\nu_\parallel}$ in the limit $y \to \infty$, in order for the $|r_A|$-dependence to cancel, and thus

$$\beta \equiv \nu_\parallel \alpha \equiv z \nu_\perp \alpha \ . \tag{2.14}$$

The above relations therefore define *three* independent critical exponents. Alternatively, the third independent exponent may be swapped for $\eta_\perp$, which characterizes how the equal-time pair correlation function decays at the critical point $r_A = 0$, $G(|\mathbf{x}|) \propto 1/|\mathbf{x}|^{d+z-2+\eta_\perp}$.

While the scaling relation (2.14) remains valid also below the upper critical dimension, which for DP turns out to be $d_c = 4$ (see Sec. III), the exponent values will become modified for $d < d_c$ as a consequence of strong fluctuation effects. Directly at the critical dimension, one expects logarithmic corrections to the above mean-field results.

The idea is now to combine several (say a number k) of such DP processes, i.e., to consider the additional reactions

$$B \to B + B \quad \text{with rate } \sigma_B \ , \tag{2.15}$$

$$B \to \emptyset \quad \text{with rate } \mu_B \ , \tag{2.16}$$

$$B + B \to B \quad \text{with rate } \lambda_B \ , \tag{2.17}$$

for particle species $B, C, \ldots$, which are coupled *unidirectionally* via the transformation reactions

$$A \to B \quad \text{with rate } \mu_{AB} \ , \tag{2.18}$$

$$A \to C \quad \text{with rate } \mu_{AC} \ , \tag{2.19}$$

$$B \to C \quad \text{with rate } \mu_{BC} \ , \tag{2.20}$$

etc., but *without feedback*, i.e., we do not allow processes of the type $B \to A$. This prescription therefore defines a *hierarchical structure* of coupled DP processes. For simplicity, we choose identical diffusion constants D on each hierarchy level.

Without the coupling reactions (2.18), ..., for each species of particles there is a continuous DP transition at $r_i = 0$, $i = A, B, \ldots$. But the situation changes in an interesting way when the transformation processes are switched on (except for species A, which is not influenced by what happens on the higher hierarchy levels). Let us first consider the simplest case of two particle species ($k = 2$) — the generalization to further hierarchy levels will then be straightforward. The mean-field rate equation (2.5) for species A remains unchanged, albeit with a modified parameter

$$r_A = (\mu_A + \mu_{AB} - \sigma_A)/D \ . \tag{2.21}$$

Notice that for the first hierarchy level, the sole effect of the transformation reactions is an increase of the total decay rate $\mu_A^{\rm tot} = \mu_A + \sum_i \mu_{Ai}$.

The rate equation for species B, however, contains a new gain term describing the feeding-in of particles via the reaction (2.18), proportional to the density of A particles present. Thus one obtains

$$\frac{\partial n_B(x,t)}{\partial t} = D\left(\nabla^2 - r_B\right) n_B(x,t) \\ -\lambda_B n_B(x,t)^2 + \mu_{AB} n_A(x,t) \ , \tag{2.22}$$

where

$$r_B = (\mu_B - \sigma_B)/D \ . \tag{2.23}$$

Notice that within the *mean-field* approximation, n_A plainly acts as an external source term. Once fluctuations are important, however, i.e., for $d < d_c = 4$, such a simple picture breaks down, especially at the multicritical point to be discussed below, where the averages and correlations of *both* $n_A(x,t)$ and $n_B(x,t)$ are governed by power laws.

We may now again search for a stationary solution n_B of Eq. (2.22), as a function of the mean-field density n_A. The general solution of the ensuing quadratic equation is

$$n_B = \left[\left(\frac{D r_B}{2\lambda_B}\right)^2 + \frac{\mu_{AB}}{\lambda_B} n_A\right]^{1/2} - \frac{D r_B}{2\lambda_B} \ . \tag{2.24}$$

Thus, for $r_A > 0$, where $n_A = 0$, one finds $n_B = D(|r_B| - r_B)/2\lambda_B$, which is zero for $r_B > 0$, and becomes equal to $n_B = D|r_B|/\lambda_B$ for $r_B < 0$. When species A is in the inactive phase, the A and B hierarchy levels are effectively decoupled, and we therefore expect an ordinary DP active / absorbing transition for species B at $r_B = 0$, as in the case $\mu_{AB} = 0$.

For $r_A < 0$, on the other hand, we have to insert (2.6) into Eq. (2.24). One may now distinguish two situations: (i) For $(D r_B/2\lambda_B)^2 \gg D|r_A|\mu_{AB}/\lambda_A\lambda_B$, we can approximate

$$n_B \approx \frac{D|r_B|}{2\lambda_B}\left[1 + \frac{D|r_A|\mu_{AB}}{2\lambda_A\lambda_B}\left(\frac{2\lambda_B}{D r_B}\right)^2\right] - \frac{D r_B}{2\lambda_B} \ , \tag{2.25}$$

and consequently for $r_B < 0$, we find that $n_B > 0$, and the B species is in its active state — the DP transition at the half line ($r_A < 0, r_B = 0$) present in the uncoupled system has disappeared (see Fig. 1). Instead, for $r_B > 0$ the terms proportional to r_B cancel in Eq. (2.25), and

$$n_B \approx |r_A|\mu_{AB}/\lambda_A r_B \ , \tag{2.26}$$

i.e., the density of species B vanishes as the critical point $r_A = 0$ of species A is approached, and with the mean-field DP exponent $\beta = 1$. Effectively, the DP critical half line ($r_A < 0, r_B = 0$) for species B has been rotated to ($r_A = 0, r_B > 0$) in the coupled system. The location of the DP critical lines for both species A and B is shown in the phase diagram of Fig. 1, where the dotted parabola

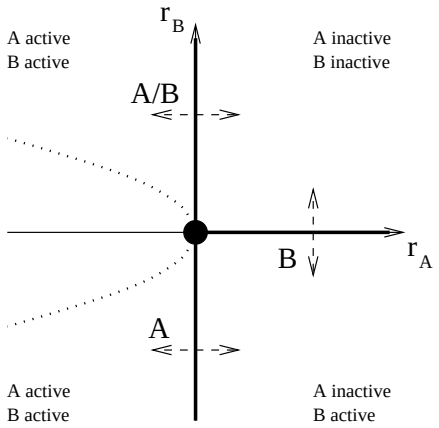

FIG. 1. Mean-field phase diagram for the two-level coupled DP process. The arrows mark DP active/absorbing transitions for the A and B particle species, respectively. The dotted parabola denotes the boundary of the multicritical regime, which includes $|r_A| = |r_B| = |r| \to 0$.

represents the boundary curve separating the two different regimes for $r_A < 0$. Notice also that in this case the "mass" terms (the contributions linear in n_A, n_B) in Eq. (2.22) vanish, and one expects both spatial and temporal power-law correlations, obviously characterized by $\nu_\perp = 1/2$ and $z = 2$. We shall later see that indeed the new critical half line ($r_A = 0, r_B > 0$) for species B is in the DP university class. Summarizing this regime, we may say that the B particles are "slaved" by the behavior of the A species.

(ii) The other regime, inside of the dotted parabola in Fig. 1, is defined by the condition $(Dr_B/2\lambda_B)^2 \ll D|r_A|\mu_{AB}/\lambda_A\lambda_B$, which includes the special case when the critical points of both hierarchy levels are approached uniformly, $|r_A| = |r_B| = |r| \to 0$. Now we can neglect the terms $\sim r_B$ in Eq. (2.24), which yields

$$n_B \approx \left(\frac{D|r_A|\mu_{AB}}{\lambda_A\lambda_B}\right)^{1/2} = \left(\frac{\mu_{AB}}{\lambda_B}\, n_A\right)^{1/2} . \qquad (2.27)$$

This implies that the density exponents on each hierarchy level i are *different* in this regime,

$$n_i \approx |r_A|^{\beta_i} , \qquad (2.28)$$

where $\beta_1 = \beta_A = 1$, and $\beta_2 = \beta_B = 1/2$ in the mean-field approximation. It is to be expected, however, that the other independent scaling exponents $\nu_\perp$ and z remain unaltered; but of course the density decay exponent at the critical point α_i will depend on the hierarchy level i, according to Eq. (2.14),

$$n_i(t) \sim t^{-\alpha_i} , \quad \alpha_i \equiv \beta_i/z\nu_\perp . \qquad (2.29)$$

Considering the two-species phase diagram (Fig. 1) again, we see that *three* critical half lines converge at the special point $r_A = r_B = 0$. The new critical behavior in this regime can therefore be interpreted as the effect of a *multicritical point* [16]. When this special point in the phase diagram is approached along a line crossing the dotted parabola in Fig. 1, one expects a *crossover* from ordinary DP to the new multicritical behavior described by the density exponents β_i and α_i. For $|r_A| = |r_B| = |r| \to 0$, the crossover features are all encoded in the generalized scaling function

$$n_B(r, \mu_{AB}, x, t) = |r|^{\beta_1} \hat{n}_A(|r|^{-\phi}\mu_{AB}/D, x/\xi_\perp, t/\xi_\parallel) , \qquad (2.30)$$

where $\xi_\perp \sim |r|^{-\nu_\perp}$ and $\xi_\parallel \sim |r|^{-\nu_\parallel}$ as in DP. This defines the *crossover exponent* ϕ, which constitutes a new scaling exponent associated with the coupling μ_{AB}. Comparing with Eq. (2.24), we identify

$$\phi = 1 \qquad (2.31)$$

within the mean-field approximation. Furthermore, we can use the above mean-field results, which, at the multicritical point, imply that $\hat{n}(y, 0, 0) \sim y^{1/2}$ for $y \to \infty$. Consequently we have

$$\beta_2 = \beta_1 - \phi/2 , \qquad (2.32)$$

which relates the new density exponent β_2 to the independent crossover exponent ϕ. Of course, Eq. (2.32) is satisfied by the mean-field values. In the fluctuation-dominated regime $d < d_c = 4$, however, there will in general be $O(\epsilon = 4 - d)$ corrections to both the critical exponents *and* the scaling functions, which will in turn lead to a modification of the scaling relation (2.32).

One may now readily generalize to higher hierarchy levels. For example, for $k = 3$, one finds the same rate equations (2.5) and (2.22) for species A and B, respectively, but where now $r_A = (\mu_A + \mu_{AB} + \mu_{AC} - \sigma_A)/D$, and $r_B = (\mu_B + \mu_{BC} - \sigma_B)/D$. The mean-field equation for $n_C(x, t)$ reads

$$\frac{\partial n_C(x,t)}{\partial t} = D\left(\nabla^2 - r_C\right) n_C(x,t) \\ -\lambda_C n_C(x,t)^2 + \mu_{BC} n_B(x,t) + \mu_{AC} n_A(x,t) , \qquad (2.33)$$

which has the general stationary solution

$$n_C = \left[\left(\frac{Dr_C}{2\lambda_C}\right)^2 + \frac{\mu_{BC}}{\lambda_C}\, n_B + \frac{\mu_{AC}}{\lambda_C}\, n_A\right]^{1/2} - \frac{Dr_C}{2\lambda_C} . \qquad (2.34)$$

A detailed analysis then reveals that, in analogy with the two-level hierarchy, there are regions in phase space where the C species evolves independently of the lower hierarchy levels. On the other hand other regimes exist where n_C is slaved by either n_A or n_B. In addition, as before, a new DP transition may arise for the C particles under appropriate conditions, when $r_A \to 0$ or $r_B \to 0$. Furthermore, the previous $k = 2$ multicritical regime occurs when either $r_A > 0$, and $|r_B| = |r_C| \to 0$ simultaneously, or $r_B > 0$, and $|r_A| = |r_C| \to 0$.

As all these features are already contained in our above investigation of the two-level coupled DP process, we restrict ourselves to the new behavior emerging for $k = 3$, when *all three* critical points coincide, i.e., $|r_A| = |r_B| = |r_C| = |r| \to 0$. More generally, in mean-field theory this multicritical regime (with altogether *seven* critical quarter planes merging at $r = 0$) is characterized by the conditions $r_A < 0$, $(Dr_B/2\lambda_B)^2 \ll D|r_A|\mu_{AB}/\lambda_A\lambda_B$ (as for $k = 2$), and $(Dr_C/2\lambda_C)^2 \ll \mu_{BC}(D|r_A|\mu_{AB}/\lambda_A\lambda_B)^{1/2}/\lambda_C + D|r_A|\mu_{AC}/\lambda_A\lambda_C$. At this special point in parameter space, n_A and n_B vanish as in Eqs. (2.6) and (2.27), respectively, while

$$n_C \approx \left(\frac{D|r|\mu_{AB}\mu_{BC}^2}{\lambda_A\lambda_B\lambda_C^2}\right)^{1/4} = \left(\frac{\mu_{BC}}{\lambda_C}\, n_B\right)^{1/2} . \quad (2.35)$$

Therefore $\beta_3 = \beta_C = 1/4$ in the mean-field approximation. Notice also that the indirect $A \to C$ transformation rate μ_{AC} does *not* enter this expression (2.35), which only depends on the coupling rates μ_{AB} and μ_{BC} between *adjacent* hierarchy levels. As the latter are not at all influenced by the presence of lower levels, this would suggest that there exists *only one* crossover exponent ϕ describing all the multicritical points generated by the unidirectional coupling of the DP processes (with $\phi = 1$ in mean-field theory).

For the density exponents, we conclude that within the mean-field approximation on hierarchy level i, using $\nu_\parallel \equiv z\nu_\perp = 1$,

$$\alpha_i = \beta_i = 1/2^{i-1} . \quad (2.36)$$

This result should describe the coupled DP multicritical point quantitatively correctly for spatial dimensions $d > d_c = 4$. Furthermore, on the mean-field level the scaling relation (2.32) generalizes to

$$\beta_i = \beta_{i-1} - \phi/2^{i-1} = \beta_1 - \phi(1 - 1/2^{i-1}) , \quad (2.37)$$

compare Eq. (2.35). Here the observation that only the direct transformation rates between neighboring hierarchy levels affect the leading contribution has entered crucially. Again, the mean-field results (2.36) and (2.31) satisfy Eq. (2.37) trivially. However, as noted above, the scaling relation (2.37) will be modified below the upper critical dimension $d_c = 4$, as a consequence of $O(\epsilon = 4 - d)$ corrections to the scaling function for the equations of state, $n_i(r)$.

III. RENORMALIZATION GROUP CALCULATIONS

A. Preliminaries

We now turn to a detailed presentation of our field-theoretic calculations. As we have pointed out in the previous sections, the effects of fluctuations invalidate a simple mean-field approach for dimensions $d < d_c = 4$. For that reason we will employ field-theoretic renormalization group methods, which allow both for a proper derivation of scaling, as well as a systematic ϵ-expansion calculation of critical exponents, below the upper critical dimension $d_c = 4$.

Our starting point for a systematic treatment of the coupled-DP reaction scheme given by (2.1)-(2.3), (2.15)-(2.18) is an appropriate master equation. On a microscopic level this comprises an exact description of the dynamics. From this equation it is then a straightforward process to derive an effective field theory: First the master equation is mapped onto a second-quantized bosonic operator representation, which is in turn mapped onto a bosonic field theory. This procedure is now standard, and we refer to Ref. [8] for further details. In our case, for the two-species coupled DP system we end up with the following action

$$\begin{aligned} S = \int d^dx \int dt \, \{ & \bar{a}\left[\partial_t + D(r_A - \nabla^2)\right] a - \sigma_A \bar{a}^2 a + \\ & + \lambda_A(\bar{a}a^2 + \bar{a}^2 a^2) - \mu_{AB}\bar{b}a + \\ & + \bar{b}\left[\partial_t + D(r_B - \nabla^2)\right] b - \sigma_B \bar{b}^2 b + \lambda_B(\bar{b}b^2 + \bar{b}^2 b^2)\} , \end{aligned} \quad (3.1)$$

where we have omitted terms related to the initial state. Aside from the taking of the continuum limit, the derivation of this action is *exact*, and in particular no assumptions regarding the precise form of the noise are required. Note that if we neglect the terms in the action (3.1) quadratic in the response fields $\bar{a}$, $\bar{b}$, then we recover a description identical to the mean-field equations (2.5) and (2.22), provided we associate the fields $a(\mathbf{x}, t)$, $b(\mathbf{x}, t)$ with the coarse-grained local densities of the A, B particles. In general, however, below the upper critical dimension $d_c = 4$, the terms quadratic in $\bar{a}$, $\bar{b}$ (corresponding to noise in a Langevin description) cannot be neglected.

It is now convenient to rescale the fields according to $\bar{a} = (\lambda_A/\sigma_A)^{1/2}\bar{\psi}_0$, $a = (\sigma_A/\lambda_A)^{1/2}\psi_0$, $\bar{b} = (\lambda_B/\sigma_B)^{1/2}\bar{\varphi}_0$, $b = (\sigma_B/\lambda_B)^{1/2}\varphi_0$, and also define new couplings $u_0 = 2(\sigma_A\lambda_A)^{1/2}$, $u_0' = 2(\sigma_B\lambda_B)^{1/2}$, as well as $\mu_0 = \mu_{AB}(\sigma_A\lambda_B/\sigma_B\lambda_A)^{1/2}$ (henceforth, the subscript "0" denotes unrenormalized quantities). If we introduce a length scale κ^{-1} and correspondingly measure times in units of κ^{-2} (i.e., $[D_0] = \kappa^0$), we find that the new fields have scaling dimension $\kappa^{d/2}$, while $[r_A] = [r_B] = [\mu_0] = \kappa^2$, which are thus relevant perturbations in the RG sense. On the other hand, $[u_0] = [u_0'] = \kappa^{2-d/2}$, and the corresponding DP non-linearities become marginal in $d_c = 4$ dimensions, as expected [13]. It is important to note, however, that $[\lambda_A] = [\lambda_B] = \kappa^{2-d}$, and hence these couplings are *irrelevant* as compared to u_0 and u_0', and may be omitted in the effective action. Finally, we set $u_0' = u_0$, such that the theory remains renormalizable with equal diffusion constants [19], and consequently arrive at

$$\begin{aligned} S_{\text{eff}} = \int d^dx \int dt \, \Big\{ & \bar{\psi}_0\left[\partial_t + D_0(r_A - \nabla^2)\right]\psi_0 - \\ & - \frac{u_0}{2}\left(\bar{\psi}_0^2\psi_0 - \bar{\psi}_0\psi_0^2\right) - \mu_0\bar{\varphi}_0\psi_0 + \end{aligned} \quad (3.2)$$

$$+\bar{\varphi}_0\left[\partial_t + D_0(r_B - \nabla^2)\right]\varphi_0 - \frac{u_0}{2}\left(\bar{\varphi}_0^2\varphi_0 - \bar{\varphi}_0\varphi_0^2\right)\Big\} \ .$$

We remark that this action is equivalent to the following set of coupled Langevin equations

$$\partial_t\psi_0 = D_0(\nabla^2 - r_A)\psi_0 - \frac{u_0}{2}\psi_0^2 + \zeta \ , \tag{3.3}$$

$$\partial_t\varphi_0 = D_0(\nabla^2 - r_B)\varphi_0 - \frac{u_0}{2}\varphi_0^2 + \mu_0\psi_0 + \eta \ , \tag{3.4}$$

which represent the obvious and expected generalizations of the mean-field equations (2.5) and (2.22), with the multiplicative Langevin noise terms

$$\langle\zeta(x,t)\zeta(x',t')\rangle = u_0\psi_0(x,t)\,\delta^d(x-x')\delta(t-t') \ , \tag{3.5}$$

$$\langle\eta(x,t)\eta(x',t')\rangle = u_0\varphi_0(x,t)\,\delta^d(x-x')\delta(t-t') \ . \tag{3.6}$$

Furthermore, for most of the analysis we will put $r_A = r_B = r_0$. There are several ways in which the effective action (3.2) can be studied. We will begin by performing our analysis in the *inactive* phase, and postpone other methods (including diagonalization and active phase computations) until later on. Inspection of the above action (3.2) reveals that, as expected, the terms involving only the ψ and $\bar{\psi}$ fields are exactly the same as in the well-known field theory for directed percolation (Reggeon field theory) [13], and their renormalization is entirely unaffected by the presence of the φ and $\bar{\varphi}$ fields. Hence we will begin by briefly reviewing the analysis of Reggeon field theory (RFT) in the inactive phase.

B. DP field theory: Inactive phase calculation

The renormalization of the RFT action is very well known (see Ref. [20]). The renormalized parameters are defined as follows:

$$\psi = Z_\psi^{1/2}\psi_0 \ , \quad \bar{\psi} = Z_\psi^{1/2}\bar{\psi}_0 \quad \tau = Z_\tau\tau_0\kappa^{-2} \ ,$$
$$D = Z_D D_0 \ , \quad u = Z_u u_0 A_d^{1/2}\kappa^{-\epsilon/2} \ , \tag{3.7}$$

with $\epsilon = 4-d$, $A_d = \Gamma(3-d/2)/2^{d-1}\pi^{d/2}$, and $\tau_0 = r_0 - r_{0c}$, where r_{0c} is the fluctuation-induced shift of the critical point. From the diagrams for the two- and three-point vertex functions (see Fig. 2), we can determine the one-loop renormalized Z factors. Using dimensional regularization and a minimal subtraction scheme, the results are

$$Z_\psi = 1 - \frac{u_0^2}{8D_0^2}\frac{A_d\kappa^{-\epsilon}}{\epsilon} \ , \tag{3.8}$$

$$Z_D = 1 + \frac{u_0^2}{16D_0^2}\frac{A_d\kappa^{-\epsilon}}{\epsilon} \ , \tag{3.9}$$

$$Z_\tau = 1 - \frac{3u_0^2}{16D_0^2}\frac{A_d\kappa^{-\epsilon}}{\epsilon} \ , \tag{3.10}$$

$$Z_u = 1 - \frac{5u_0^2}{16D_0^2}\frac{A_d\kappa^{-\epsilon}}{\epsilon} \ , \tag{3.11}$$

with r_{0c} given by the recursive equation

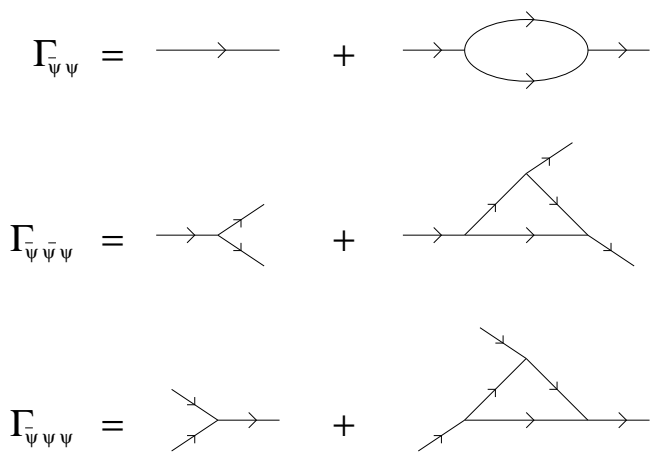

FIG. 2. Diagrams for the two- and three-point vertex functions to one-loop order for the pure DP field theory.

$$r_{0c} = -\frac{u_0^2}{4D_0^2}\int_p \frac{1}{r_{0c}+p^2} \ , \tag{3.12}$$

where we have used the abbreviation $\int_p \ldots = \int \ldots d^dp/(2\pi)^d$. Defining the flow functions $\zeta_u = \kappa\partial_\kappa \ln(u/u_0)$ etc., and with an effective coupling $v = u^2/16D^2$, the RG β function has the form

$$\beta_v = \kappa\partial_\kappa v = 2v(\zeta_u - \zeta_D) = v(-\epsilon + 12v) \ , \tag{3.13}$$

giving a stable, non-trivial fixed point $v^* = \epsilon/12 + O(\epsilon^2)$.

The appropriate renormalization group equation for the renormalized field $\langle\psi_R\rangle$, where the angular brackets denote averaging with respect to the RFT action, is

$$\left(\kappa\frac{\partial}{\partial\kappa} + \zeta_\tau\tau\frac{\partial}{\partial\tau} + \zeta_D D\frac{\partial}{\partial D} + \zeta_v v\frac{\partial}{\partial v} - \frac{1}{2}\zeta_\psi\right) \times\langle\psi_R(\kappa,\tau,D,v,x,t)\rangle = 0 \ . \tag{3.14}$$

Defining the dimensionless field $\hat{\psi}$ as

$$\langle\psi_R(\kappa,\tau,D,v,x,t)\rangle = \kappa^{d/2}\hat{\psi}(\tau,v,\kappa x,\kappa^2 Dt) \ , \tag{3.15}$$

the solution of (3.14), obtained by means of the method of characteristics $\kappa \to \kappa\ell$, when the coupling v has run to its fixed point value v^* is

$$\langle\psi_R(\kappa,\tau,D,v,x,t)\rangle = \kappa^{d/2}\ell^{(d-\zeta_\psi^*)/2} \times\hat{\psi}(\tau\ell^{\zeta_\tau^*}, v^*, \kappa x\ell, \kappa^2 Dt\ell^{2+\zeta_D^*}) \ . \tag{3.16}$$

By inserting the matching condition $\ell = |\tau|^{-1/\zeta_\tau^*}$, we can now *derive* the scaling relation (2.13) quoted in the previous section. At the fixed point, we obtain

$$\langle\psi_R(\kappa,\tau,D,v,x,t)\rangle = |\tau|^\beta\hat{\psi}\left(v^*, \frac{\kappa x}{|\tau|^{-\nu_\perp}}, \frac{\kappa^2 Dt}{|\tau|^{-\nu_\parallel}}\right) \ , \tag{3.17}$$

where the exponents can be identified as combinations of the ζ functions evaluated at the non-trivial fixed point:

$$\eta_\perp = -\zeta_D^* - \zeta_\psi^* = -\frac{\epsilon}{12} + O(\epsilon^2) \ , \tag{3.18}$$

$$\nu_\perp = \frac{1}{-\zeta_\tau^*} = \frac{1}{2} + \frac{\epsilon}{16} + O(\epsilon^2) \ , \tag{3.19}$$

$$\nu_\parallel = \frac{2+\zeta_D^*}{-\zeta_\tau^*} = 1 + \frac{\epsilon}{12} + O(\epsilon^2) \ , \tag{3.20}$$

$$z = \frac{\nu_\parallel}{\nu_\perp} = 2 + \zeta_D^* = 2 - \frac{\epsilon}{12} + O(\epsilon^2) \ , \tag{3.21}$$

$$\beta = \frac{d-\zeta_\psi^*}{-2\zeta_\tau^*} = \frac{\nu_\perp}{2}(d+z-2+\eta_\perp)$$
$$= 1 - \frac{\epsilon}{6} + O(\epsilon^2) \ . \tag{3.22}$$

Directly at the upper critical dimension $d_c = 4$ ($\epsilon = 0$), the power laws with these critical exponents are replaced with logarithmic corrections to the mean-field results $\eta_\perp = 0$, $\nu_\perp = 1/2$, $\nu_\parallel = 1$, $z = 2$, and $\beta = 1$ (see also Ref. [21]). The flow equation for $v(\ell)$ becomes $\ell\, dv(\ell)/d\ell = \beta_v(\ell) = 12v(\ell)^2$, which is solved by $v(\ell) = v[1 - 12v\ln\ell]^{-1}$, where $v = v(\ell = 1)$. Similarly, $\ell\, dD(\ell)/d\ell = \zeta_D(\ell)D(\ell) = -vD(\ell)[1-12v\ln\ell]^{-1}$ has the solution $D(\ell) = D[1-12v\ln\ell]^{1/12}$, and $\ell\, d\tau(\ell)/d\ell = \zeta_\tau(\ell)\tau(\ell) = (-2 + 3v[1-12v\ln\ell]^{-1})\tau(\ell)$ is solved by $\tau(\ell) = \tau\ell^{-2}[1-12v\ln\ell]^{-1/4}$. We now integrate the flow equations until $|\tau(\ell)| = 1$, or $\ell \sim |\tau|^{1/2}(-\ln|\tau|)^{-1/8}$. This yields immediately the divergence of both the correlation length $\xi_\perp$ and the characteristic time scale $\xi_\parallel$ upon approaching the phase transition,

$$\xi_\perp \sim \ell^{-1} \approx |\tau|^{-1/2}(-\ln|\tau|)^{1/8} \ , \tag{3.23}$$

$$\xi_\parallel \sim \ell^{-2}D(\ell)^{-1} \approx |\tau|^{-1}(-\ln|\tau|)^{1/6} \ . \tag{3.24}$$

In order to obtain the corresponding logarithmic correction for the density exponent β, we employ the solution (3.16) of the RG equation and the mean-field result (2.6), and find

$$\langle\psi_R(\kappa,\tau,D,v)\rangle \sim \kappa^{d/2}\ell^{d/2}C(\ell)^{-1/2}\frac{|\tau(\ell)|}{v(\ell)^{1/2}} \ , \tag{3.25}$$

where $C(\ell) = \exp(\int_1^\ell \zeta_\psi(\ell')d\ell'/\ell')$, or equivalently, $\ell dC(\ell)/d\ell = \zeta_\psi(\ell)C(\ell) = 2vC(\ell)[1-12v\ln\ell]^{-1}$, with the solution $C(\ell) = [1-12v\ln\ell]^{-1/6}$. Combining everything, and setting $d = 4$ in Eq. (3.25) finally yields

$$\langle\psi_R\rangle \sim |\tau|(-\ln|\tau|)^{1/3} \ . \tag{3.26}$$

Notice that we had to take care and keep track of the dangerous irrelevant variable v here.

C. Coupled DP field theory: Inactive phase

We now return to the renormalization of the coupled DP field theory. Right from the outset we must take into account one key feature of the full theory — namely that, on physical grounds, one expects the generation of *additional* mixed cubic vertices. Physically, these novel vertices correspond to the additionally generated processes

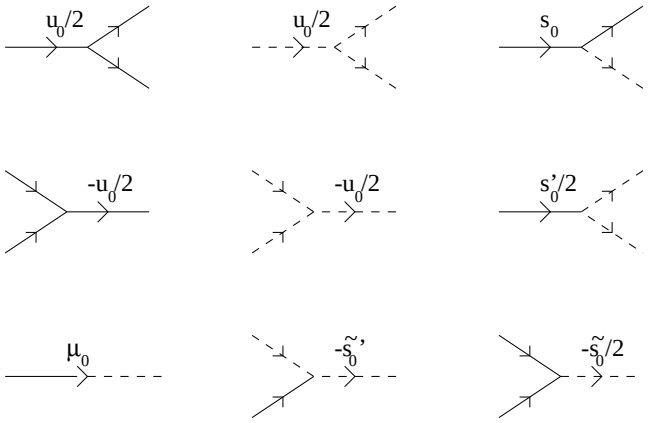

FIG. 3. The vertices of the full action $S_{\rm mc}$.

$A \to A + B$, $A \to B + B$, $A + A \to B$, and $A + B \to A$, with rates σ_{AB}, σ'_{AB}, λ_{AB}, and λ'_{AB}, say. These vertices must be introduced from the very beginning, and hence we have to replace the above action (3.2) with $S_{\rm mc} = S_{\rm eff} + \Delta S$, where

$$\Delta S = \int d^dx \int dt \ \Big[-s_0\bar\varphi_0\bar\psi_0\psi_0 - \frac{s'_0}{2}\bar\varphi_0^2\psi_0 + \frac{\tilde s_0}{2}\bar\varphi_0\psi_0^2 + \tilde s'_0\bar\varphi_0\varphi_0\psi_0 \Big] \ . \tag{3.27}$$

Note that in the shifted theory used above, the new reaction processes also modify the bare parameters r_A, μ_0, and u_0, and furthermore lead to the identification $s_0 \sim \sigma_{AB} \geq 0$, $s'_0 \sim \sigma'_{AB} \geq 0$, $\tilde s_0 \sim -\lambda_{AB} \leq 0$, and $\tilde s'_0 \sim \lambda'_{AB} \geq 0$. In the effective Langevin-type description, Eqs. (3.3)-(3.6) are then replaced by

$$\partial_t\psi_0 = D_0(\nabla^2 - r_A)\psi_0 - \frac{u_0}{2}\psi_0^2 + \zeta \ , \tag{3.28}$$

$$\partial_t\varphi_0 = D_0(\nabla^2 - r_B)\varphi_0 - \frac{u_0}{2}\varphi_0^2 - \frac{\tilde s_0}{2}\psi_0^2 - \tilde s'_0\psi_0\varphi_0 + \mu_0\psi_0 + \eta \ , \tag{3.29}$$

where the noise terms satisfy

$$\zeta(x,t) = a\xi_1(x,t), \tag{3.30}$$

$$\eta(x,t) = b\xi_2(x,t) + c\xi_1(x,t) \ . \tag{3.31}$$

Here ξ_1 and ξ_2 are uncorrelated white noise variables of variance one, and the coefficients a, b and c satisfy:

$$a^2 = u_0\psi_0, \tag{3.32}$$

$$b^2 = u_0\varphi_0 + \left(s'_0 - \frac{s_0^2}{u_0}\right)\psi_0, \tag{3.33}$$

$$c^2 = \frac{s_0^2}{u_0}\psi_0. \tag{3.34}$$

The complete vertices of the full action $S_{\rm mc}$ are depicted in Fig. 3. The propagators for the ψ and φ fields are denoted by solid and dashed lines, respectively. The next

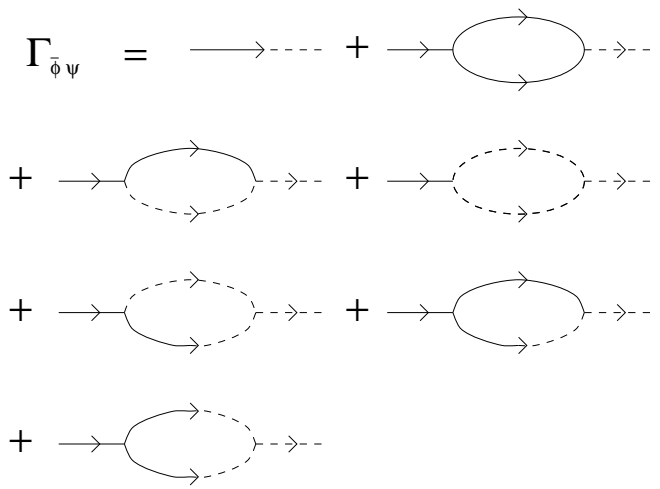

FIG. 4. "Mixed" two-point vertex function $\Gamma_{\bar{\varphi}\psi}$ to one-loop order for the coupled DP field theory.

task is to compute the renormalized couplings and RG fixed points of the full theory. To begin with, we notice that the DP couplings in the action (3.2) are renormalized in the same way as in RFT, i.e., the factors $Z_\psi = Z_\varphi$, Z_τ, Z_D, and Z_u are *identical* with those in Eqs. (3.8)–(3.11). Hence we can conclude that the stable fixed points for the dimensionless renormalized coupling $u = Z_u u_0 A_d^{1/2} \kappa^{-\epsilon/2}$ reads as in DP:

$$v^* = [(u/4D)^*]^2 = \epsilon/12 + O(\epsilon^2) \ . \tag{3.35}$$

For this reason, the critical exponents $\eta_\perp$, $\nu_\perp$ and z remain those of the DP universality class for the second hierarchy level (i.e., for the B species), and in fact for higher hierarchy levels as well.

However, the same will *not* be true for the exponents β_i (for $i > 1$). For example, the exponent β_2 *is* affected by the renormalization of μ_0, and hence only the exponent β_1 will remain the same as in DP. In order to compute the renormalization of μ_0, we must consider the diagrams renormalizing the "mixed" two-point vertex function $\Gamma_{\bar{\varphi}\psi}$, as depicted in Fig. 4. At the normalization point $q = \omega = 0$, $\tau = 1$, we find

$$\Gamma^{\rm NP}_{\bar{\varphi}\psi} = -\mu_0 \left[1 - \frac{u_0(s_0 + \tilde{s}_0')}{4D_0^2} \int_p \frac{1}{(\kappa^2 + p^2)^2} - \frac{u_0^2 \mu_0}{8 D_0^3} \int_p \frac{1}{(\kappa^2 + p^2)^3} - \frac{2 s_0 \tilde{s}_0' + u_0(s_0' + \tilde{s}_0)}{4 D_0 \mu_0} \int_p \frac{1}{\kappa^2 + p^2} \right] \ . \tag{3.36}$$

Notice that the integral in the last term of (3.36) diverges in $d = 2$. In the same way as in the shift of the percolation threshold in DP, see Eq. (3.12), we may take care of this UV divergence by means of an additive renormalization, and then multiplicatively renormalize the UV poles in $d = 4$. Thus, defining the dimensionless renormalized coupling

$$\mu = Z_\mu (\mu_0 - \mu_{0c}) \kappa^{-2} \ , \tag{3.37}$$

with the associated flow function $\zeta_\mu = \kappa \partial_\kappa \ln(\mu/\mu_0)$, we have

$$\mu_{0c} = \frac{2 s_0 \tilde{s}_0' + u_0(s_0' + \tilde{s}_0)}{4 D_0} \int_p \frac{1}{\kappa^2 + p^2} \ , \tag{3.38}$$

and

$$(Z_\psi Z_\varphi)^{1/2} Z_\mu = 1 - \frac{u_0(s_0 + \tilde{s}_0')}{4 D_0^2} \int_p \frac{1}{(\kappa^2 + p^2)^2} - \frac{u_0^2 \mu_0}{8 D_0^3} \int_p \frac{1}{(\kappa^2 + p^2)^3} \ . \tag{3.39}$$

We will later see that the prefactor multiplying the shift μ_{0c} in Eq. (3.38), which involves the various mixed three-point couplings, actually vanishes in an appropriate parameter subspace containing *both* emerging fixed lines, see below. In principle, additional additive renormalizations would be required to render $\partial_{q^2} \Gamma^{\rm NP}_{\bar{\varphi}\psi}$ and $\partial_\omega \Gamma^{\rm NP}_{\bar{\varphi}\psi}$ UV-finite [19]. These counterterms, to be added to the action (3.2), would be of the form

$$\int d^d x \int dt \, \bar{\varphi} \left(A \partial_t - B \nabla^2 \right) \psi \ . \tag{3.40}$$

However, as both A and B are again proportional to the prefactor of the integral in Eq. (3.38), they all vanish at the fixed lines to be discussed later. A subtle point which can be raised concerning these counterterms is the stability of the scaling behavior of the theory (in other words the stability of the fixed lines to be derived later on) against the introduction of a term like Eq. (3.40) into the original action (3.2). After this paper was submitted for publication, Janssen [22] has shown that indeed the scaling behavior is unaffected by the introduction of such terms, and thus μ_0 is the only mixed coupling constant that needs to be introduced.

Note also that the final diagram in Fig. 4 [see the second lines of Eqs. (3.36) and (3.39)] is UV-finite in $d = 4$, and so for the moment we shall neglect it in a *minimal* subtraction scheme (this is, however, a somewhat subtle point in the active phase, which will be discussed in more detail in Sec. III F). Certainly, for $\mu \ll 1$, i.e., in an additional expansion in the transmutation rate μ, this diagram is suppressed as compared to the other contributions. We then find

$$Z_\mu = 1 + \left(\frac{u_0^2}{8 D_0^2} - \frac{u_0(s_0 + \tilde{s}_0')}{4 D_0^2} \right) \frac{A_d \kappa^{-\epsilon}}{\epsilon} \ , \tag{3.41}$$

and after defining $g = s/D$ and $\tilde{g}' = \tilde{s}'/D$, we have

$$\begin{aligned} \zeta_\mu &= -2 - 2v + \sqrt{v}(g + \tilde{g}') \\ &= -2 - \frac{\epsilon}{6} + \frac{1}{2} \sqrt{\frac{\epsilon}{3}} \, (g^* + \tilde{g}'^*) \ , \end{aligned} \tag{3.42}$$

where in the second line we have inserted the DP fixed point (3.35).

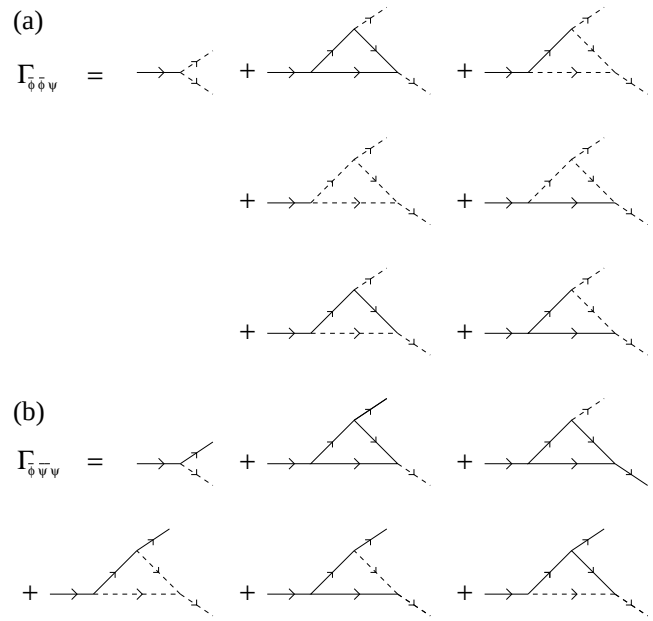

FIG. 5. The "mixed" three-point vertex functions (a) $\Gamma_{\bar\varphi\bar\varphi\psi}$, and (b) $\Gamma_{\bar\varphi\bar\psi\psi}$, to one-loop order.

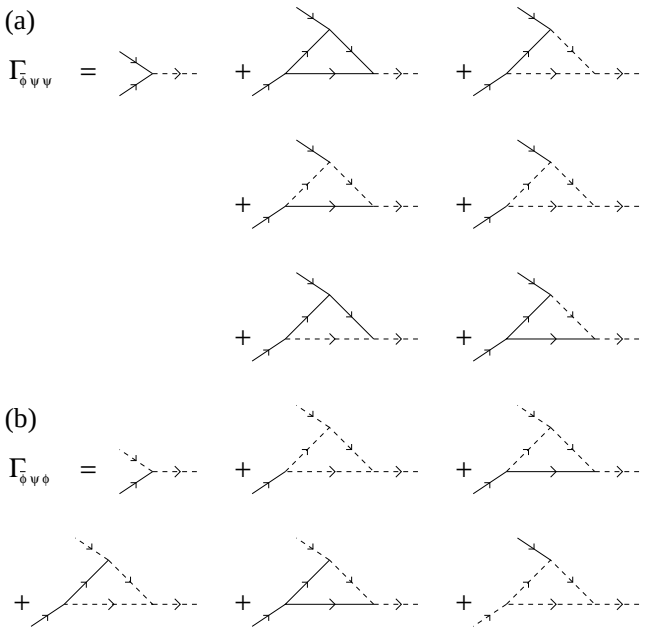

FIG. 6. The "mixed" three-point vertex functions (a) $\Gamma_{\bar\varphi\psi\psi}$, and (b) $\Gamma_{\bar\varphi\psi\varphi}$ to one-loop order.

An inspection of Eq. (3.36) now shows that, in order to compute the renormalization of μ_0, we must first consider the renormalization of the various mixed three-point couplings,

$$s = Z_s s_0 A_d^{1/2}\kappa^{-\epsilon/2}\ , \quad s' = Z_{s'} s'_0 A_d^{1/2}\kappa^{-\epsilon/2}\ ,$$
$$\tilde s = Z_{\tilde s}\tilde s_0 A_d^{1/2}\kappa^{-\epsilon/2}\ , \quad \tilde s' = Z_{\tilde s'}\tilde s'_0 A_d^{1/2}\kappa^{-\epsilon/2}\ . \qquad (3.43)$$

Evaluating first the renormalization of s', which can be calculated from the diagrams shown in Fig. 5(a), we find

$$\Gamma^{NP}_{\bar\varphi\bar\varphi\psi_R} = \frac{-s' A_d^{-1/2}\kappa^{\epsilon/2}}{Z_\psi^{1/2} Z_\varphi Z_{s'}}\left[1 - \left(\frac{u_0 s_0\tilde s_0}{s'_0} + u_0 s_0 + u_0^2 \right.\right.$$
$$\left.\left. + u_0\tilde s'_0 + \frac{u_0 s_0\tilde s'_0}{s'_0} + \frac{s_0^2\tilde s'_0}{s'_0}\right)\frac{1}{2D_0^2}\int_p \frac{1}{(\kappa^2+p^2)^2}\right]\ . \qquad (3.44)$$

Inserting the appropriate expressions for Z_ψ and Z_φ from Eq. (3.8) and using $\int_p (\kappa^2+p^2)^{-2} = A_d\kappa^{-\epsilon}/\epsilon$, we end up with

$$Z_{s'} = 1 + \left[-\frac{5u_0^2}{16D_0^2} - \frac{u_0 s_0}{2D_0^2} - \frac{u_0 s_0\tilde s_0}{2s'_0 D_0^2}\right.$$
$$\left. - \frac{u_0\tilde s'_0}{2D_0^2} - \frac{u_0 s_0\tilde s'_0}{2s'_0 D_0^2} - \frac{s_0^2\tilde s'_0}{2s'_0 D_0^2}\right]\frac{A_d\kappa^{-\epsilon}}{\epsilon}\ . \qquad (3.45)$$

Similarly, with the aid of the diagrams shown in Fig. 5(b) and Fig. 6, we can compute the Z factors for the other mixed three-point couplings,

$$Z_s = 1 + \left[-\frac{u_0^2}{16D_0^2} - \frac{u_0 s_0}{4D_0^2} - \frac{u_0^2\tilde s_0}{4s_0 D_0^2}\right.$$
$$\left. - \frac{u_0\tilde s'_0}{2D_0^2}\right]\frac{A_d\kappa^{-\epsilon}}{\epsilon}\ , \qquad (3.46)$$

$$Z_{\tilde s} = 1 + \left[-\frac{5u_0^2}{16D_0^2} - \frac{u_0 s_0}{2D_0^2} - \frac{u_0\tilde s'_0}{2D_0^2}\right.$$
$$\left. - \frac{u_0\tilde s'_0 s_0}{2\tilde s_0 D_0^2} - \frac{u_0 s'_0\tilde s'_0}{2\tilde s_0 D_0^2} - \frac{\tilde s'^2_0 s_0}{2\tilde s_0 D_0^2}\right]\frac{A_d\kappa^{-\epsilon}}{\epsilon}\ , \qquad (3.47)$$

$$Z_{\tilde s'} = 1 + \left[-\frac{u_0^2}{16D_0^2} - \frac{u_0^2 s'_0}{4\tilde s'_0 D_0^2} - \frac{u_0 s_0}{4D_0^2}\right.$$
$$\left. - \frac{u_0\tilde s'_0}{4D_0^2}\right]\frac{A_d\kappa^{-\epsilon}}{\epsilon}\ . \qquad (3.48)$$

We note in passing that, in principle, a product of the quartic vertices [which we previously discarded from the action (3.1)] and μ_0 might also enter the renormalizations of the three-point functions. However, we have checked that these additional couplings all have negative RG eigenvalues and are therefore irrelevant.

With the definitions $g = s/D$, $g' = s'/D$, $\tilde g = \tilde s/D$ and $\tilde g' = \tilde s'/D$, it is now straightforward to compute the RG β functions for these new variables. Since we have $\beta_g = \kappa\partial_\kappa g = g(\zeta_s - \zeta_D)$ etc., where $\zeta_s = \kappa\partial_\kappa \ln(s/s_0)$ etc., we find to one-loop order

$$\beta_g = -\frac{\epsilon}{3}(g-\tilde g) + \sqrt{\frac{\epsilon}{3}}g\left(\frac{1}{2}g + \tilde g'\right)\ , \qquad (3.49)$$

$$\beta_{g'} = \sqrt{\frac{\epsilon}{3}}g(g'+\tilde g) + \sqrt{\frac{\epsilon}{3}}\tilde g'(g+g') + \frac{1}{2}g^2\tilde g'\ , \qquad (3.50)$$

$$\beta_{\tilde g} = \sqrt{\frac{\epsilon}{3}}g(\tilde g+\tilde g') + \sqrt{\frac{\epsilon}{3}}\tilde g'(g'+\tilde g) + \frac{1}{2}\tilde g'^2 g\ , \qquad (3.51)$$

$$\beta_{\tilde g'} = \frac{\epsilon}{3}(g'-\tilde g') + \sqrt{\frac{\epsilon}{3}}\tilde g'\left(g + \frac{1}{2}\tilde g'\right)\ , \qquad (3.52)$$

where we have already inserted the one-loop fixed point value for $v^* = [(u/4D)^*]^2$. Notice the symmetry of the

above RG β functions with respect to exchanging $g \leftrightarrow \tilde{g}'$ and $g' \leftrightarrow \tilde{g}$. We now search for fixed-point solutions of the above equations where $\beta_g^* = \beta_{g'}^* = \beta_{\tilde{g}}^* = \beta_{\tilde{g}'}^* = 0$. Using Eqs. (3.49) and (3.52) to eliminate $\tilde{g}$ and g' from the remaining two β functions, the above system of equations can be solved exactly. After some tedious algebra, we find two *fixed-line* solutions, the first one being

$$g^* = -\tilde{g}'^*, \quad \tilde{g}^* - g'^* = 2g^* \ ,$$
$$g^{*2} = 2\sqrt{\frac{\epsilon}{3}}(g^* + g'^*) \ . \tag{3.53}$$

Computing the eigenvalues of the stability matrix

$$\frac{\partial \beta_\gamma}{\partial \delta} \ , \quad \text{with} \quad \{\gamma\}, \{\delta\} = \{g, g', \tilde{g}, \tilde{g}'\} \ , \tag{3.54}$$

yields the eigenvalues 0, 0, $-\epsilon/3$, $-\epsilon/3$. Hence, this first fixed line, which includes the Gaussian fixed points for the mixed three-point couplings, is *unstable*. The second fixed line is given by

$$g'^* = \tilde{g}^*, \quad g^* + \tilde{g}'^* = 2\sqrt{\frac{\epsilon}{3}} \ ,$$
$$g^{*2} = 2\sqrt{\frac{\epsilon}{3}}(g^* + g'^*) \ , \tag{3.55}$$

with stability matrix eigenvalues 0, $\epsilon/3$, $\epsilon/3$, $4\epsilon/3$. Hence this second fixed line is *stable*. Notice also that *both* of the above fixed lines satisfy the condition

$$\sqrt{\frac{\epsilon}{3}}(g'^* + \tilde{g}^*) = -g^* \tilde{g}'^* \ , \tag{3.56}$$

which ensures the cancellation of the strongly singular (UV-divergent in $d = 2$) diagrams for the renormalization of μ_0 in Eq. (3.36).

We can now insert the values of $g^* + \tilde{g}'^*$ at the two fixed lines (3.53) and (3.55), respectively, into Eq. (3.42), and thus obtain

$$\zeta_\mu^* = \begin{cases} -2 + \epsilon/6 + O(\epsilon^2) & \text{(stable line)} \ , \\ -2 - \epsilon/6 + O(\epsilon^2) & \text{(unstable line)} \ . \end{cases} \tag{3.57}$$

We are now in a position to *derive* the scaling form (2.30) for the B species density, postulated in the previous section. We begin by writing down the renormalization group equation for the renormalized field $\langle \varphi_R \rangle$, where the angular brackets denote averaging with respect to the full action $S_{\rm mc}$

$$\left(\kappa \frac{\partial}{\partial \kappa} + \zeta_\tau \tau \frac{\partial}{\partial \tau} + \zeta_D D \frac{\partial}{\partial D} + \zeta_v v \frac{\partial}{\partial v} + \right.$$
$$+ \zeta_g g \frac{\partial}{\partial g} + \zeta_{g'} g' \frac{\partial}{\partial g'} + \zeta_{\tilde{g}} \tilde{g} \frac{\partial}{\partial \tilde{g}} + \zeta_{\tilde{g}'} \tilde{g}' \frac{\partial}{\partial \tilde{g}'} \tag{3.58}$$
$$\left. + \zeta_\mu \mu \frac{\partial}{\partial \mu} - \frac{1}{2}\zeta_\varphi \right) \langle \varphi_R(\kappa, \tau, D, v, \{g\}, \mu, x, t) \rangle = 0 \ ,$$

and where we have used the notation $\{g\} = \{g, g', \tilde{g}, \tilde{g}'\}$. Defining the dimensionless field $\hat{\varphi}$ as

$$\langle \varphi_R(\kappa, \tau, D, v, \{g\}, \mu, x, t) \rangle = \kappa^{d/2} \times \hat{\varphi}(\tau, v, \{g\}, \mu/D, \kappa x, \kappa^2 D t) \ , \tag{3.59}$$

the solution of Eq. (3.58) when the couplings $v, \{g\}$ have run to their fixed-point/line values is

$$\langle \varphi_R(\kappa, \tau, D, v, \{g\}, \mu, x, t) \rangle = \kappa^{d/2} \ell^{(d - \zeta_\varphi^*)/2} \times \hat{\varphi}\left(\tau \ell^{\zeta_\tau^*}, v^*, \{g^*\}, (\mu/D) \ell^{\zeta_\mu^* - \zeta_D^*}, \right.$$
$$\left. \kappa x \ell, \kappa^2 D t \ell^{2 + \zeta_D^*} \right) \ . \tag{3.60}$$

Inserting the matching condition $\ell = |\tau|^{-1/\zeta_\tau^*}$, and dropping the $v, \{g\}$ couplings, we obtain

$$\langle \varphi_R(\kappa, \tau, D, \mu, x, t) \rangle \propto |\tau|^{-(d - \zeta_\varphi^*)/2\zeta_\tau^*} \times \hat{\varphi}\left((\mu/D) |\tau|^{-(\zeta_\mu^* - \zeta_D^*)/\zeta_\tau^*}, \kappa x |\tau|^{-1/\zeta_\tau^*}, \right.$$
$$\left. \kappa^2 D t |\tau|^{-(2 + \zeta_D^*)/\zeta_\tau^*} \right) \ . \tag{3.61}$$

Identifying $\beta_1 = \beta = -(d - \zeta_\varphi^*)/2\zeta_\tau^*$, $\nu_\perp = -1/\zeta_\tau^*$, $\nu_\parallel = -(2 + \zeta_D^*)/\zeta_\tau^*$ and defining the crossover exponent as $\phi = (\zeta_\mu^* - \zeta_D^*)/\zeta_\tau^*$, we have

$$\langle \varphi_R(\kappa, \tau, D, \mu, x, t) \rangle \propto |\tau|^{\beta_1} \hat{\varphi}\left(\frac{\mu/D}{|\tau|^\phi}, \frac{\kappa x}{|\tau|^{-\nu_\perp}}, \frac{\kappa^2 D t}{|\tau|^{-\nu_\parallel}} \right) \ , \tag{3.62}$$

in agreement with the scaling hypothesis (2.30) postulated in the previous section. Using our earlier results for the ζ^* functions, we find

$$\phi = \begin{cases} 1 + O(\epsilon^2) & \text{(stable line)} \ , \\ 1 + \epsilon/6 + O(\epsilon^2) & \text{(unstable line)} \ . \end{cases} \tag{3.63}$$

Notice the absence of $O(\epsilon)$ contributions to ϕ at the stable fixed line, which is due to remarkable cancellations. This of course also implies that there are no logarithmic corrections to the crossover exponent ϕ in $d_c = 4$ dimensions.

The final step in this calculation is now to compute the exponent β_2. Unfortunately, in order to do this, we must first understand the behavior of the scaling function (3.62) in the active phase. As we shall see, it contributes non-trivial corrections to the exponent β_2 at $O(\epsilon)$. Hence it is *not* sufficient simply to match the scaling function to that calculated in mean-field theory [23] — such a procedure would miss these $O(\epsilon)$ corrections. However, before dealing further with this active phase calculation for the B species, we first discuss the simpler problem of pure DP in the active phase, which also applies to the first level (the A particles) of the coupled DP problem.

D. DP field theory: Active phase calculation

In this section, we will review the one-loop calculation of the expectation value of the field in the active phase

for the case of a single field, i.e., the case of (decoupled) directed percolation. In this way we can obtain an expression for the critical exponent $\beta_1 = \beta$ [24].

We start with the action for a single field (see Sec. III A)

$$S_{\rm DP} = \int d^dx \int dt \, \left\{ \bar\psi_0 \left[\partial_t + D_0(r_0 - \nabla^2) \right] \psi_0 - \right. \\ \left. - \frac{u_0}{2} \left(\bar\psi_0^2 \psi_0 - \bar\psi_0 \psi_0^2 \right) \right\} \ . \quad (3.64)$$

In the active phase ($r_0 < 0$) the expectation value of the field ψ_0 is non-zero, and we define a shifted field ψ_{c0} by

$$\psi_0 = v_0 \ + \ \psi_{c0} \ , \quad (3.65)$$

to obtain the new action

$$S'_{\rm DP} = \int d^dx \int dt \, \left\{ \bar\psi_0 (\partial_t \psi_{c0} - D_0 \nabla^2 \psi_{c0} + D_0 r_0 \psi_{c0}) + \right. \\ + \bar\psi_0 (D_0 r_0 v_0 + \frac{1}{2} u_0 v_0^2) - \frac{1}{2} u_0 v_0 \bar\psi_0^2 + u_0 v_0 \bar\psi_0 \psi_{c0} + \\ \left. + \frac{1}{2} u_0 (\psi_{c0} - \bar\psi_0) \bar\psi_0 \psi_{c0} \right\} \ . \quad (3.66)$$

We now fix v_0 by equating the coefficient of $\bar\psi_0$ to zero. Thus

$$v_0 = -\frac{2 D_0 r_0}{u_0} = \frac{2 D_0 |r_0|}{u_0} \ , \quad (3.67)$$

where v_0 is the classical (mean-field) value of the expectation value of the field. Substituting these values into Eq. (3.66), we obtain

$$S'_{\rm DP} = \int d^dx \int dt \, \left[\bar\psi_0 (\partial_t \psi_{c0} - D_0 \nabla^2 \psi_{c0} + D_0 |r_0| \psi_{c0}) + \right. \\ \left. + \frac{1}{2} u_0 (\psi_{c0} - \bar\psi_0) \bar\psi_0 \psi_{c0} - D_0 |r_0| \bar\psi_0^2 \right] \ . \quad (3.68)$$

In the following we will define $\tau_0 \equiv -r_0$. From Eq. (3.65) it follows that

$$\langle \psi_0 \rangle = v_0 \ + \ \langle \psi_{c0} \rangle \ . \quad (3.69)$$

There is only one diagram contributing to the expectation value $\langle \psi_{c0} \rangle$ to one-loop order, and it is depicted in Fig. 7. We thus find, using dimensional regularization,

$$\langle \psi_0 \rangle = \frac{2 D_0 \tau_0}{u_0} - \frac{1}{2} \frac{u_0}{D_0} \int_p \frac{1}{p^2 + \tau_0} \\ = \frac{2 D_0 \tau_0}{u_0} - \frac{u_0}{D_0} \frac{\Gamma(1 - d/2)}{(8\pi)^{d/2}} (2\tau_0)^{d/2 - 1} \ . \quad (3.70)$$

Using the relations between the bare and renormalized quantities given in Eqs. (3.7)–(3.11), the last expression yields

$$\langle \psi_R \rangle = \frac{2 D \tau}{u} A_d^{1/2} \kappa^{d/2} Z_\psi^{1/2} Z_u Z_\tau^{-1} Z_D^{-1} \\ \times \left(1 + \frac{u^2}{4 \epsilon D^2} \frac{\tau^{\epsilon/2}}{1 - \epsilon/2} \right) \ . \quad (3.71)$$

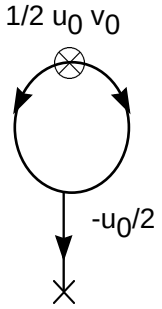

FIG. 7. One-loop diagram for $\langle \psi_{c0} \rangle$ in the pure DP active phase calculation.

We see that all the poles in ϵ cancel out as they should. At the fixed point $(u/D)^* = 2(\epsilon/3)^{1/2}$, we finally find to leading order in ϵ,

$$\langle \psi_R \rangle = 2 \left(\frac{D}{u} \right)^* A_d^{1/2} \kappa^{d/2} (1 + \epsilon/6) \ \tau \ \left(1 - \frac{\epsilon}{6} \ln \tau \right) \ . \quad (3.72)$$

Upon exponentiating the logarithm, assuming that this can be done unambiguously, we see that

$$\langle \psi_R \rangle = n_A \sim \tau^{1 - \epsilon/6} \ , \quad (3.73)$$

which implies $\beta_1 = \beta = 1 - \epsilon/6 + O(\epsilon^2)$, as already cited in Eq. (3.22), where the scaling relation $\beta = \nu_\perp (d + z - 2 + \eta_\perp)/2$ was employed.

E. Coupled DP field theory: Active phase

We now proceed to discuss the active phase calculation for two coupled fields, as represented by the action $S_{\rm mc} = S_{\rm eff} + \Delta S$ given in Eqs. (3.2) and (3.27). We will again restrict our discussion to the case where $r_A = r_B = r_0$. Based on the mean-field analysis of Sec. II, we anticipate that the expectation values of the fields are different from zero when $r_0 < 0$. Hence we define the shifted fields

$$\psi_0 = v_{A0} + \psi_{c0} \ , \quad (3.74)$$
$$\bar\psi_0 = \bar\psi_{c0} \ , \quad (3.75)$$
$$\varphi_0 = v_{B0} + \varphi_{c0} \ , \quad (3.76)$$
$$\bar\varphi_0 = \bar\varphi_{c0} \ . \quad (3.77)$$

The new action expressed in terms of the shifted fields will now involve terms linear in $\bar\psi_{c0}$ and $\bar\varphi_{c0}$. Equating the coefficients of these terms to zero fixes the constants v_{A0} and v_{B0} to be the classical (mean-field) values. These are determined by the equations

$$D_0 r_0 v_{A0} + \frac{1}{2} u_0 v_{A0}^2 = 0 \ , \quad (3.78)$$
$$D_0 r_0 v_{B0} + \frac{1}{2} u_0 v_{B0}^2 - \mu_0 v_{A0} + \frac{1}{2} \tilde s_0 v_{A0}^2 + \tilde s'_0 v_{A0} v_{B0} = 0 \ .$$

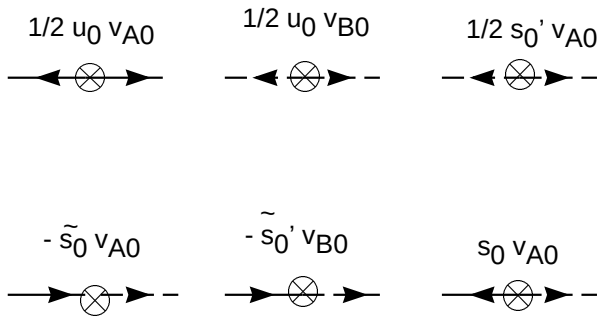

FIG. 8. New two-point vertices in the active phase coupled DP calculation.

The solutions of these equations are

$$v_{A0} = \frac{2D_0|r_0|}{u_0} \ , \tag{3.79}$$

$$v_{B0} = \sqrt{\frac{4\mu_0 D_0|r_0|}{u_0^2}} + O(|r_0|) \ . \tag{3.80}$$

The fields now have new masses given by

$$D_0 r_{A0} = D_0 r_0 + u_0 v_{A0} = D_0|r_0| \ , \tag{3.81}$$

$$D_0 r_{B0} = D_0 r_0 + u_0 v_{B0} + \tilde{s}_0' v_{A0} \tag{3.82}$$

$$\simeq \sqrt{4\mu_0 D_0|r_0|} + O(|r_0|) \ . \tag{3.83}$$

There are also various new two-point vertices as depicted in Fig. 8, whose corresponding terms in the action are given by

$$\int d^dx \int dt \left[-\frac{1}{2} u_0 v_{A0} \bar{\psi}_{c0}^2 - \frac{1}{2}(u_0 v_{B0} + s_0' v_{A0}) \bar{\varphi}_{c0}^2 - \right.$$
$$\left. -(\mu_0 - \tilde{s}_0 v_{A0} - \tilde{s}_0' v_{B0}) \bar{\varphi}_{c0} \psi_{c0} - s_0 v_{A0} \bar{\varphi}_{c0} \bar{\psi}_{c0} \right] \ . \tag{3.84}$$

We can now proceed with the calculation of the expectation value of the second field φ_0, by using Eq. (3.76) and computing $\langle \varphi_{c0} \rangle$ to one-loop order. The full calculation is unnecessarily complicated, and universality dictates that we can calculate the critical behavior for *any* point on the stable fixed line. However, we note that the unstable and stable fixed lines do not necessarily have to give the same critical behavior, and indeed in our case we will find that they do not.

For the stable fixed line, we have actually performed the calculation in two different ways. Both methods yield identical results, and this provides us with an important extra check on our methods. In the first approach we have chosen a subspace of initial parameters

$$s_0 = \tilde{s}_0', \ s_0' = \tilde{s}_0 \ , \tag{3.85}$$

with the stable fixed point $(u/D)^* = 2\sqrt{\epsilon/3}$, $g^* = \tilde{g}'^* = -2g'^* = -2\tilde{g}^* = \sqrt{\epsilon/3}$. In the second approach we have chosen

$$s_0' = \tilde{s}_0 = \tilde{s}_0' = 0 \ , \tag{3.86}$$

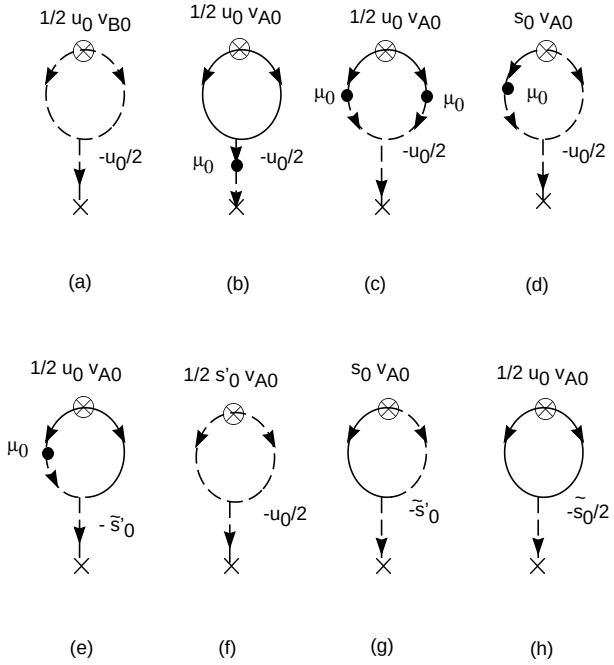

FIG. 9. One-loop diagrams for the computation of $\langle \varphi_{c0} \rangle$ in the coupled DP active phase calculation.

and with the stable fixed point $(u/D)^* = 2\sqrt{\epsilon/3}$, $g^* = (s/D)^* = 2\sqrt{\epsilon/3}$, $g'^* = \tilde{g}^* = \tilde{g}'^* = 0$.

Note that both the parameter subspaces given by Eqs. (3.85) and (3.86) are closed under renormalization flows, as is evident from a close inspection of the RG β functions given by Eqs. (3.49), (3.50), (3.51) and (3.52). The first choice is the more natural one for investigating the multicritical point, since when Eq. (3.85) is satisfied the original action $S_{\rm mc} = S_{\rm eff} + \Delta S$ is invariant under a generalization of the usual DP 'rapidity reversal', namely

$$\psi_0(x,t) \longleftrightarrow -\bar{\varphi}_0(x,-t) \ , \tag{3.87}$$

$$\bar{\psi}_0(x,t) \longleftrightarrow -\varphi_0(x,-t) \ , \tag{3.88}$$

and under renormalization this symmetry is preserved. However, the calculation using the condition (3.86) is somewhat simpler. In both approaches the unstable (non-trivial) fixed point is given by $(u/D)^* = 2\sqrt{\epsilon/3}$, and $g^* = g'^* = \tilde{g}^* = \tilde{g}'^* = 0$.

The diagrams contributing to the expectation value of $\langle \varphi_{c0} \rangle$ to one-loop order are depicted in Fig. 9. We will outline first the calculation using the second approach described above. In that case diagrams (e) through (h) vanish and one has to consider only the first four diagrams. We thus find to one-loop order, after implementing Eq. (3.86),

$$\langle \varphi_0 \rangle = v_{B0} - \frac{u_0^2 v_{B0}}{2D_0 r_{B0}} I_1(r_{B0}) - \frac{u_0^2 v_{A0}\mu_0}{2D_0^2 r_{A0} r_{B0}} I_1(r_{A0})$$
$$- \frac{u_0^2 v_{A0}\mu_0^2}{2D_0 r_{B0}} I_2(r_{A0},\, r_{B0}) - \frac{u_0 s_0 v_{A0}\mu_0}{D_0 r_{B0}} I_3(r_{B0};\, r_{A0}, r_{B0})$$
$$+ \cdots \ . \tag{3.89}$$

With the use of dimensional regularization, the various integrals appearing in Eq. (3.89) are given by the following expressions

$$I_1(a) = \frac{1}{2D_0}\int_p \frac{1}{p^2+a} = -\frac{A_d}{D_0\epsilon(2-\epsilon)}\, a^{1-\epsilon/2}, \quad (3.90)$$

$$I_2(a,b) = \frac{1}{4D_0^3}\int_p \frac{1}{(p^2+a)(p^2+b)(p^2+\frac{a+b}{2})} \quad (3.91)$$
$$= -\frac{A_d}{D_0^3\epsilon(2-\epsilon)}\frac{1}{(a-b)^2}\left[a^{1-\epsilon/2}+b^{1-\epsilon/2}- \right.$$
$$\left. -2\left(\frac{a+b}{2}\right)^{1-\epsilon/2}\right],$$

$$I_3(b;a,b) = \frac{1}{4D_0^2}\int_p \frac{1}{(p^2+b)(p^2+\frac{a+b}{2})} \quad (3.92)$$
$$= \frac{A_d}{2D_0^2\epsilon(2-\epsilon)}\left[\frac{a+b}{a-b}\left(\frac{a+b}{2}\right)^{-\epsilon/2}+ \right.$$
$$\left. +\frac{2b}{b-a}b^{-\epsilon/2}\right] .$$

We are interested in obtaining the ϵ expansions of the above expressions in the regime where $b \gg a$ (since $r_{B0} \gg r_{A0}$ as $r_0 \to 0$). In that case we find

$$I_1(a) \approx -\frac{A_d\kappa^{-\epsilon}}{2D_0\epsilon}\left(1+\frac{\epsilon}{2}\right)a\left(1-\frac{\epsilon}{2}\ln\frac{a}{\kappa^2}\right)+\cdots ,$$
$$I_2(a,b) \approx \frac{A_d\kappa^{-\epsilon}}{4D_0^3}\frac{\ln 2}{b}+\cdots , \quad (3.93)$$
$$I_3(b;a,b) \approx \frac{A_d\kappa^{-\epsilon}}{4D_0^2\epsilon}\left(1+\frac{\epsilon}{2}-\frac{\epsilon}{2}\ln 2\right)\left(1-\frac{\epsilon}{2}\ln\frac{b}{\kappa^2}\right)+$$
$$+\cdots .$$

Let us postpone for the time being a full discussion of the term containing I_2, i.e. the contribution from diagram (c) in Fig. 9. Notice that this term is ultraviolet finite, i.e. it does not involve a pole in ϵ. However, after using expression (3.93) it appears to contribute a (negative) constant to the expectation value of φ. This seems problematic and a full discussion of this point will be given in the next section.

We now define again

$$\tau_0 = -(r_0 - r_{0c}) , \quad (3.94)$$

where to first order in standard perturbation theory we have

$$r_{0c} = -\frac{u_0^2}{4D_0^2}\int_p \frac{1}{p^2} . \quad (3.95)$$

This integral vanishes in dimensional regularization, and hence in the following calculation we will ignore r_{0c}, as was done in the pure DP active phase computation. When using the relations between the bare and renormalized quantities in Eqs. (3.7) and (3.37), we find to leading order in an expansion in τ:

$$\langle\varphi_R\rangle \approx \frac{2\sqrt{\mu D\tau}}{u}A_d^{1/2}\kappa^{d/2}Z_\varphi^{1/2}Z_u Z_\mu^{-1/2}Z_\tau^{-1/2}Z_D^{-1/2}$$
$$\times\left[1+\frac{u^2}{4D^2\epsilon}(1+\epsilon/2)\left(1-\frac{\epsilon}{4}\ln\frac{4\mu\tau}{D}\right)+\right.$$
$$+\frac{u^2}{8D^2\epsilon}(1+\epsilon/2)\left(1-\frac{\epsilon}{2}\ln\tau\right)- \quad (3.96)$$
$$\left.-\frac{us}{8D^2\epsilon}(1+\epsilon/2-\epsilon\ \ln 2/2)\left(1-\frac{\epsilon}{4}\ln\frac{4\mu\tau}{D}\right)+\cdots\right] .$$

A check reveals that all the poles in ϵ cancel, as they should. At the fixed point given by $(u/D)^* = (s/D)^* = 2\sqrt{\epsilon/3}$, we find

$$\langle\varphi_R\rangle \approx 2\left(\frac{D}{u}\right)^*\left(1+\frac{\epsilon}{6}\right)\sqrt{\frac{\mu\tau}{D}} \quad (3.97)$$
$$\times\left(1-\frac{\epsilon}{12}\ln(\mu\tau/D)-\frac{\epsilon}{12}\ln\tau+\frac{\epsilon}{24}\ln(\mu\tau/D)+\ldots\right) .$$

Assuming that only one such scaling term becomes generated, we may now exponentiate the logarithms, and see that

$$\langle\varphi_R\rangle \sim \tau^{1/2-\epsilon/8}(\mu/D)^{1/2-\epsilon/24}$$
$$= \tau^{1-\epsilon/6}\left(\tau^{-1}\mu/D\right)^{1/2-\epsilon/24} , \quad (3.98)$$

from which we infer

$$\beta_2 = \frac{1}{2}-\frac{\epsilon}{8}+O(\epsilon^2) , \quad (3.99)$$
$$\phi = 1+O(\epsilon^2) , \quad (3.100)$$

where ϕ is the crossover exponent, a result consistent with that derived previously in the inactive phase. We also see that in the definition

$$\langle\varphi_R\rangle = \tau^{\beta_1}\widehat{\varphi}(\tau^{-\phi}\mu/D), \quad (3.101)$$

the scaling function behaves for large argument as

$$\widehat{\varphi}(x) \sim x^{1/2-\epsilon/24}, \quad (3.102)$$

a result that differs from the mean-field behavior at $O(\epsilon)$. At the upper critical dimension $d_c = 4$, a comparison with Eq. (3.26) for the first hierarchy level suggests the logarithmic correction

$$\langle\varphi_R\rangle \sim \tau^{1/2}(-\ln\tau)^{1/4} . \quad (3.103)$$

Let us also discuss briefly the calculation using the approach given by Eq. (3.85) above. In that case we have an additional four diagrams (e)-(h) to consider. However, we will see that diagrams (f)-(h) contribute to higher-order terms in an expansion in τ, beyond the leading behavior described above. Diagram (e) gives an equal contribution to diagram (d), but since the value of s at the corresponding fixed point is half of what it was in the previous calculation, the final result is exactly the same. To verify these claims we observe that diagrams (e) to (h) contribute the following additional terms to the r.h.s. of Eq. (3.89),

$$-\frac{u_0 s_0 v_{A0}\mu_0}{2D_0 r_{B0}} I_3(r_{A0}; r_{B0}, r_{A0}) - \frac{u_0 s_0^{'} v_{A0}}{2D_0 r_{B0}} I_1(r_{B0}) -$$
$$-\frac{s_0^2 v_{A0}}{D_0 r_{B0}} I_4(r_{A0}, r_{B0}) - \frac{u_0 s_0^{'} v_{A0}}{2D_0 r_{B0}} I_1(r_{A0}) \ . \qquad (3.104)$$

The only new integral I_4 is given by

$$I_4(a,b) = I_1((a+b)/2) \ . \qquad (3.105)$$

It is now easy to verify that the last three terms give a contribution of $O(\tau_0)$ and higher which can be neglected in comparison with the $O(\sqrt{\tau_0})$ terms which we have kept. The I_3 contribution in the first term is given by

$$I_3(a;b,a) = \frac{A_d}{2D_0^2\epsilon(2-\epsilon)} \left[\frac{b+a}{b-a} \left(\frac{a+b}{2} \right)^{-\epsilon/2} + \frac{2a}{a-b} a^{-\epsilon/2} \right].$$
$$\approx \frac{A_d}{4D_0^2\epsilon} \left(1 + \frac{\epsilon}{2} + \frac{\epsilon}{2}\ln 2\right) \left(1 - \frac{\epsilon}{2}\ln b\right) + \cdots \ , \qquad (3.106)$$

and thus diagram (e) yields essentially the same contribution as diagram (d). Since the value of $(s/D)^*$ is now one-half of its value in the previous approach, our final result follows.

Finally, let us discuss the behavior at the unstable, non-trivial fixed point given by $(u/D)^* = 2\sqrt{\epsilon/3}$, and $g^* = g'^* = \tilde{g}^* = \tilde{g}'^* = 0$. Returning to Eq. (3.96), with the last term set equal to zero, we have

$$\langle \varphi_R \rangle \propto \sqrt{\frac{\mu\tau}{D}} \left(1 - \frac{\epsilon}{12}\ln(\mu\tau/D) - \frac{\epsilon}{12}\ln\tau + \ldots\right) \ , \qquad (3.107)$$

to leading order. Exponentiating the logarithms (again with the assumption mentioned above) we find

$$\langle \varphi_R \rangle \sim \tau^{1/2-\epsilon/6} (\mu/D)^{1/2-\epsilon/12} \qquad (3.108)$$

$$= \tau^{1-\epsilon/6} \left(\tau^{-1-\epsilon/6}\mu/D\right)^{1/2-\epsilon/12} \ , \qquad (3.109)$$

and thus in this case $\beta_2 = 1/2 - \epsilon/6 + O(\epsilon^2)$, $\phi = 1 + \epsilon/6 + O(\epsilon^2)$ and the scaling function $\hat{\varphi}(x) \sim x^{1/2-\epsilon/12+O(\epsilon^2)}$ for large values of the argument.

F. Technical difficulties

We now return to diagram (c) of Fig. 9. Substituting the expression for $I_2(a,b)$ from Eq. (3.93) into the corresponding expression in Eq. (3.89), we find that the contribution of diagram (c) to the expectation value of $\langle \varphi_0 \rangle$ is:

$$-\frac{u_0^2 A_d \kappa^{-\epsilon} v_{A0}}{8 D_0^4 r_{B0}^2} \mu_0^2 \ln 2 \to -\kappa^{d/2} A_d^{1/2} \left(\frac{u}{D}\right)^* \frac{\ln 2}{16} \frac{\mu}{D}, \qquad (3.110)$$

to leading order in ϵ and in an expansion in powers of $\sqrt{\tau}$. This is in contrast to our expectation (backed up by our simulation results in Sec. IV) that $\langle \varphi \rangle$ should vanish at the transition as $\tau \to 0$. Notice that this diagram is ultraviolet-finite and hence there are no poles in ϵ. On the other hand, the loop integral $I_2(a,b)$ is infrared-*divergent* for any $d \leq 6$, which leads to the behavior $I_2(a,b) \propto 1/b$ for $d = 4$ when $a \to 0$. One can argue that for $d > 4$ the prefactor of this diagram will vanish due to the fact that u flows to the Gaussian fixed point $u^* = 0$. But for $d < 4$ we seem to have a problem, the origin of which is obviously the appearance of the strongly *relevant* parameter μ as an effective coupling (two-point vertex) in the perturbation expansion.

This difficulty is somewhat reminiscent of the random-field problem, where infrared-divergent diagrams in perturbation theory lead to a shift in the upper critical dimension in a φ^4 theory from 4 to 6 [25]. This is due to the extra propagators in a given loop as compared to the pure case. One might perhaps argue that because of the unidirectionality of the interaction between the two fields ψ and φ, the ψ field acts as a spatially and temporally correlated random field from the point of view of the φ field, since there is no backwards feedback, meaning that the φ field has no influence on the ψ field. However, in contrast to the random field case, where the random field is taken to be of constant variance as one approaches the transition temperature, the expectation value of the ψ field vanishes as one approaches the multicritical point, and this seems to soften the effect of the infrared problem. Another marked difference is that ψ is not a quenched random variable in the traditional sense, since it is displaying strong temporal fluctuations in the multicritical regime. Since the above infrared-divergent integral becomes tamed at $d = 6$, one might think that, similar to the random-field problem, one might control its divergence by a dimensionality shift. However, we have not been able to construct a sensible field theory for this problem by choosing $d = 6$ as the upper critical dimension. Actually other infrared-divergent diagrams can be found at higher loop orders, which are even more divergent than the diagram just mentioned, as in, e.g., Fig. 10(a). IR-divergent diagrams also appear in the expansion of other vertex functions, like the $\varphi\overline{\varphi}^2$ vertex to one-loop order, where one can easily construct diagrams with one or two insertions of the ψ field into the φ-triangular diagram, see Fig. 10(b),(c).

Another place were a similar diagram appears is in the "mixed" vertex function $\Gamma_{\overline{\varphi}\psi}$, see the last diagram of Fig. 4 and Eq. (3.36). If we evaluate this vertex function at a general "temperature" τ, rather than at $\tau = 1$ as in Eq. (3.36), we find that its contribution in $d = 4$ diverges like $1/\tau$ as $\tau \to 0$. From the active phase side, the same diagram diverges like $1/\sqrt{\mu\tau}$. This prevents one from defining the renormalized μ parameter at criticality as the value of this function for $\tau = 0$, at least not at $q = \omega = 0$. One can attempt to absorb this divergence by a finite (non-ultraviolet divergent) renormalization addition to Z_μ, which will then become temperature depen-

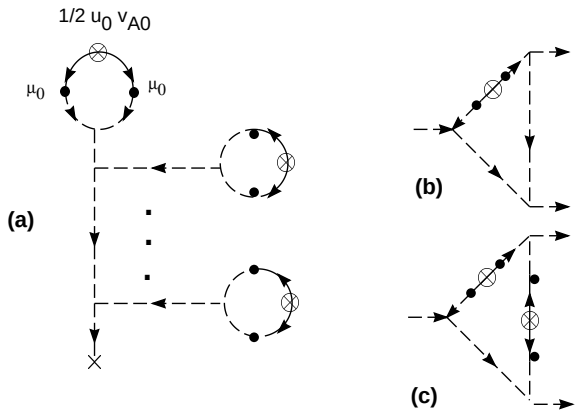

FIG. 10. (a) An IR-divergent diagrams at higher loop order, contributing to the expectation value of φ. (b) IR-divergent diagram contributing to the three-point vertex function with one insertion of $\bar{\psi}^2$. (c) IR-divergent diagram contributing to the three-point vertex function with two insertions of $\bar{\psi}^2$.

dent. Thus one would define Z_μ such that the renormalized $\Gamma_{\overline{\varphi}\psi}$ evaluated at $q = \omega = 0$ would be finite as $\tau \to 0$. If this is done in the active phase we have verified that it cancels the contribution of the problematic contribution to $\langle\varphi_0\rangle$ against the corresponding term in Z_μ. However, this procedure appears somewhat artificial and not entirely satisfactory since it requires a temperature-dependent renormalization constant. Also, to establish such a renormalization scheme, one would have to check that this procedure works properly to higher loop orders as well, where even more IR-divergent contributions are present.

In the absence of a truly satisfactory resolution of the infrared difficulty, one might argue that its effect is to render the ϵ expansion derived in the previous sections invalid. Yet, this conclusion is too far reaching, since even if a well-defined field theory that describes the asymptotic critical behavior of all hierarchy levels is problematic (and may even not exist), our results are still likely to be valid for a range of the parameter τ close to the transition point, as will become clear from the following reasoning.

We notice that the problematic IR-divergent diagrams are proportional to higher powers of the inter-species coupling μ. For example, the IR-problematic diagram mentioned at the beginning of this section gives an overall contribution proportional to μ, whereas the other diagrams contributing to $\langle\varphi\rangle$ to one loop order (which were mentioned at the end of the previous section) are proportional to $\sqrt{\mu}$ or $\sqrt{\mu}\ln\mu$. For small values of μ these problematic diagrams are therefore suppressed. Now μ is a relevant coupling in the RG sense and thus the effective (running) coupling increases as one goes deeper into the critical region. But by starting with an initially small value of μ, one can increase the size of the region in which μ remains small. In this intermediate region the IR-divergent diagrams can still be neglected and the scaling results obtained in the previous sections are valid. Thus, our theory predicts that for small μ, as τ is decreased, one can observe a scaling regime where the critical behavior is characterized by the universal exponents calculated in the previous sections. In particular the exponent β_2 should be observable. Ultimately, as τ becomes very small the field theory may break down. However, we cannot exclude the emergence of another non-trivial asymptotic scaling regime deep in the critical region. The ensuing scaling behavior might possibly be extracted by isolating the structure of the leading IR divergences to all orders and then by a resummation of the ill-defined perturbative expansion in μ. However although this possibility exists, it cannot be substantiated at this point by more rigorous arguments. What is more likely to happen is that a *non-universal* crossover behavior ensues (non-universal as a consequence of the breakdown of the ϵ expansion and hence the RG construction), which eventually terminates in asymptotically decoupled DP behavior. In other words, the B species are no longer slaved to the A particles, but rather behave independently such that their density vanishes with a power β_1. This is supported by the simulation results, as will be discussed in a later section. Probably, at sufficiently large times, the discrete and finite number of A particles already vanishes in the interior of comparatively large domains. Consequently the B particles, which were actually generated previously through the reaction $A \to B$, interact and annihilate as if they were independent and decoupled from the A species. Further discussions of this issue in the light of the simulation results will follow at the end of the paper.

G. Diagonalized theory

We now return to another of the approaches to the coupled DP problem mentioned in Sec. III A, namely that of diagonalizing the action (3.2) to remove the quadratic cross-term linking the ψ_0 and φ_0 fields. If we apply the transformations

$$\begin{aligned}\Phi_0 &= \varphi_0 + \frac{\mu_0}{D_0(r_A - r_B)}\psi_0 \ , \\ \bar{\Psi}_0 &= \bar{\psi}_0 - \frac{\mu_0}{D_0(r_A - r_B)}\bar{\varphi}_0 \ ,\end{aligned} \tag{3.111}$$

then the action (3.2) is transformed to

$$\begin{aligned}S_{\rm diag} = \int d^dx \int dt \Big\{ &\bar{\Psi}_0 \left[\partial_t + D_0(r_A - \nabla^2)\right]\psi_0 - \\ &- \frac{u_0}{2}\left[\bar{\Psi}_0^2\psi_0 - \bar{\Psi}_0\psi_0^2\right] + \\ +\bar{\varphi}_0 &\left[\partial_t + D_0(r_B - \nabla^2)\right]\Phi_0 - \frac{u_0}{2}\left[\bar{\varphi}_0^2\Phi_0 - \bar{\varphi}_0\Phi_0^2\right] - \\ -S_0\bar{\varphi}_0\bar{\Psi}_0\psi_0 &+ \tilde{S}_0'\bar{\varphi}_0\Phi_0\psi_0 + \frac{\tilde{S}_0}{2}\bar{\varphi}_0\psi_0^2 - \frac{S_0'}{2}\bar{\varphi}_0^2\psi_0 \Big\} \ .\end{aligned} \tag{3.112}$$

Here we have defined

$$
\begin{aligned}
S_0 &= \frac{u_0\mu_0}{D_0(r_A - r_B)} \ , \\
\tilde{S}_0' &= -\frac{u_0\mu_0}{D_0(r_A - r_B)} \ , \\
\frac{\tilde{S}_0}{2} &= \frac{\mu_0}{2D_0(r_A - r_B)}\left(u_0 + \frac{u_0\mu_0}{D_0(r_A - r_B)}\right) \ , \\
\frac{S_0'}{2} &= \frac{-\mu_0}{2D_0(r_A - r_B)}\left(u_0 - \frac{u_0\mu_0}{D_0(r_A - r_B)}\right) \ .
\end{aligned}
\tag{3.113}
$$

Notice that this new action (3.112) has precisely the form of our original full action $S_{\rm mc}$, except that the quadratic cross-term which linked the ψ_0 and φ_0 fields has been eliminated. This renders the diagonalized model a special case of the very general quadratically coupled DP processes studied by Janssen [15]. In addition, we remark that this diagonalizing transformation breaks down when $r_A = r_B$, consistent with our earlier identification of novel multicritical behavior for $r_A = r_B = r \to 0$.

Since the action (3.112) is very similar to $S_{\rm mc}$, we can quickly determine its ensuing scaling behavior. The mixed three-point vertices have exactly the same fixed-line structure as derived in Sec. III C. Thus the diagrams which would have generated a quadratic cross-term under renormalization (i.e., the $d = 2$ UV-divergent diagrams in Fig. 4) cancel out at *both* of the fixed lines (at least to one-loop order). Hence, to this order, the DP parts of the action for the ψ and Φ fields are entirely unaffected by the presence of the mixed three-point vertices, generated by the transformation (3.111). In that case we expect pure DP behavior on the transition lines away from the multicritical point, as we had earlier anticipated, and as shown on very general grounds in Ref. [15].

H. Crossover theory

Outside the multicritical regime, the mean-field approximation suggested that we should expect ordinary DP critical behavior for the B species, if either $\tau_A > 0$ and $\tau_B \to 0$, or $\tau_B > 0$ and $\tau_A \to 0$, see Fig. 1. If one starts near the multicritical point where both $\tau_A \to 0$ and $\tau_B \to 0$, then at first the multicritical density exponent β_2 should be observed, eventually crossing over to the ordinary DP exponent β_1, and similarly for the exponents α_i, etc. In the first crossover region $\tau_A > 0$ and $\tau_B \to 0$, indicated by the dashed arrow B in Fig. 1, this scenario is rather obvious on the mean-field level, valid for $d > d_c$: Here, the density $n_A = 0$, and therefore the coupling between the different hierarchy levels vanishes. Our study of the diagonalized theory in the preceding Sec. III G established the DP character of the ensuing active/absorbing transition at $\tau_B = 0$ even below d_c, when fluctuations become dominant.

The more interesting case is the situation for $\tau_B > 0$ and $\tau_A \to 0$, where there exists a DP phase transition for the A particles. For $\mu_{AB} > 0$, we argued above that the B species becomes "slaved" to the critical A species, and is driven to a non-equilibrium phase transition itself as the A control parameter $\tau_A \to 0$. In order to describe the ensuing crossover scenario, we apply the generalized minimal subtraction scheme of Ref. [26], where we retain the parameter τ_B in the RG flow equations, and use $\tau_A = 1$ as the normalization point. The Z factors then become functions of the non-linear couplings *and* τ_B. In order to simplify the calculation, we once again use the reduced parameter space where $g' = \tilde{g} = \tilde{g}' = 0$. However, now we must distinguish between the non-linear DP coupling v for the A species, and the one for the B particles, which we denote with v'. The remaining important Wilson RG functions then become

$$\zeta_{\tau_A} = -2 + 3v \ , \tag{3.114}$$

$$\zeta_{\tau_B} = -2 + \frac{3v'}{(1+\tau_B)^{1+\epsilon/2}} \ , \tag{3.115}$$

$$\zeta_\mu - \zeta_D = -2 - v + \frac{\sqrt{v'}g}{(1+\tau_B)^{1+\epsilon/2}} \ , \tag{3.116}$$

and the RG β functions for the couplings v, v', and g read

$$\beta_v = v\left(-\epsilon + 12v\right) \ , \tag{3.117}$$

$$\beta_{v'} = v'\left(-\epsilon + \frac{12v'}{(1+\tau_B)^{1+\epsilon/2}}\right) \ , \tag{3.118}$$

$$\beta_g = g\left(-\frac{\epsilon}{2} + 2v + \frac{\sqrt{v'}g}{(1+\tau_B)^{1+\epsilon/2}}\right) \ . \tag{3.119}$$

Of course, the A species DP fixed point remains $v^* = \epsilon/12$ with $\zeta^*_{\tau_A} = -2 + \epsilon/4$. However, the *effective* B coupling $v'(\ell)/[1+\tau_B(\ell)]^{1+\epsilon/2} \to 0$ asymptotically as $\ell \to 0$ (since $v'(\ell) \sim \ell^{-\epsilon}$) and hence $\tau_B(\ell) \sim \ell^{-2}$ according to Eqs. (3.118) and (3.115). Thus $\beta_g \to -(\epsilon/3)g$, and $g(\ell) \to 0$ as well. Consequently, $\zeta^*_\mu - \zeta^*_D = -2 - \epsilon/12$, and we recover

$$\phi = (\zeta^*_\mu - \zeta^*_D)/\zeta^*_{\tau_A} = 1 + \epsilon/6 + O(\epsilon^2) \ , \tag{3.120}$$

i.e., the result given in Eq. (3.63) at the unstable fixed line. Notice that here the critical exponents for the B species are given by $\nu_\perp = -1/\zeta^*_{\tau_A}$ etc., and thus take on the usual DP values (3.19) to (3.22).

In the active phase, we may confirm this by direct calculation, as in Secs. III D and III E. From the diagrams in Fig. 9, for finite τ_B, and in essentially the reduced parameter space, only graph (b) survives. After inserting the p_c shift, and multiplying by the appropriate renormalization constants (in the generalized minimal subtraction scheme), the equation of state in terms of the renormalized quantities assumes the form

$$
\begin{aligned}
\langle\varphi_R\rangle\tau_B|\tau_A|\left[1 - \frac{4v}{\epsilon}\left(1 + \frac{\epsilon}{2} - \frac{\epsilon}{2}\ln|\tau_A|\right)\right] \sim \\
\sim 2\sqrt{v}\frac{\mu}{D}\langle\psi_R\rangle^2 \ .
\end{aligned}
\tag{3.121}
$$

At the DP fixed point $v^* = \epsilon/12$, we exponentiate the logarithm on the left-hand side to $|\tau_A|^{1-\epsilon/6} = \tau_A^{\beta_1}$, and use $\langle\psi_R\rangle \sim \tau_A^{\beta_1}$, which leads us to

$$\langle\varphi_R\rangle \sim 2\sqrt{v^*}\,\frac{\mu}{D}\,\frac{\tau_A^{\beta_1}}{\tau_B}\ , \tag{3.122}$$

which obviously generalizes the mean-field result (2.26).

I. Higher hierarchy levels

We end this section on applications of the renormalization group to coupled DP with some remarks on the behavior of higher hierarchy levels $i > 2$. As pointed out already in Sec. II, while generically the transitions from the active to the absorbing inactive phase of particle species i are of the DP universality class, with the critical density exponent β_1, one finds the two-level hierarchy exponent β_2 whenever the first two critical points coincide, $r_A = r_B$. However, further special multicritical behavior appears at higher levels if additional r_k become equal. In mean-field theory, one has $\beta_i = 1/2^{i-1}$ for $r_1 = \ldots = r_i$. In the two-level hierarchy ($i = 2$) multicritical regime, one finds a strong *downward* renormalization of β_1 and β_2 due to fluctuations, see Eqs. (3.22) and (3.99).

In order to see what happens at higher hierarchy levels, let us briefly consider the three-species coupled DP process in the vicinity of the multicritical regime, and for small transmutation rates. Notice that in this situation fluctuations will not only generate the vertices corresponding to Eq. (3.27) on each adjacent level, but also the indirect transmutation $A \to C$, as well as all possible three-point vertices *unidirectionally* coupling the levels (and in principle additional higher order non-linearities, which however turn out to be irrelevant). In order to simplify the analysis, we merely use the reduced parameter space analogous to keeping only the new vertex s_0 in the two-level process. This leaves us with the following effective action (with the fields $\bar\phi_0$ and ϕ_0 describing the particle species C),

$$\begin{aligned} S_{\rm eff} = \int d^dx \int dt \Big\{ & \bar\psi_0 \left[\partial_t + D_0(r_A - \nabla^2)\right]\psi_0 - \\ & -\frac{u_0}{2}\left(\bar\psi_0^2\psi_0 - \bar\psi_0\psi_0^2\right) + \\ & +\bar\varphi_0\left[\partial_t + D_0(r_B - \nabla^2)\right]\varphi_0 - \frac{u_0}{2}\left(\bar\varphi_0^2\varphi_0 - \bar\varphi_0\varphi_0^2\right) - \\ & -\mu_0\bar\varphi_0\psi_0 - s_0\bar\varphi_0\bar\psi_0\psi_0 + \\ & +\bar\phi_0\left[\partial_t + D_0(r_C - \nabla^2)\right]\phi_0 - \frac{u_0}{2}\left(\bar\phi_0^2\phi_0 - \bar\phi_0\phi_0^2\right) - \\ & -\mu_0'\bar\phi_0\varphi_0 - t_0\bar\phi_0\bar\varphi_0\varphi_0 - \\ & -\bar\mu_0\bar\phi_0\psi_0 - \bar t_0\bar\phi_0\bar\psi_0\psi_0 - \rho_0\bar\phi_0\bar\varphi_0\psi_0 \Big\}\ . \end{aligned} \tag{3.123}$$

Clearly, if we just consider the B/C reactions, then a fully analogous calculation as in Sec. III C yields

$$\zeta_{\mu'} - \zeta_D = -2 - v + \sqrt{v}\,h\ , \tag{3.124}$$

where $h = t/D$. Hence with $v^* = \epsilon/12$, the crossover exponent at the associated two-level multicritical point is

$$\phi' = (\zeta^*_{\mu'} - \zeta^*_D)/\zeta^*_\tau = 1 + O(\epsilon^2)\ , \tag{3.125}$$

computed at the stable fixed point $h^* = 2\sqrt{\epsilon/3}$ (which is the remnant of the stable fixed line in the reduced parameter space). We may wonder now if the unidirectional, sequential coupling of three hierarchy levels leads to a further novel crossover exponent associated with the transmutation $A \to C$. Thus, we compute the renormalization of the vertex function $\Gamma_{\bar\phi\psi}$, which leads to

$$\zeta_{\bar\mu} - \zeta_D = -2 - v + \sqrt{v}\,(f + \bar f)\ , \tag{3.126}$$

where $f = \bar t/D$ and $\bar f = \rho\mu'/D\bar\mu$. We now merely need the renormalizations of both f and $\bar f$. In just the same manner as in the two-level calculation, one finds from the renormalization of $\Gamma_{\bar\phi\bar\psi\psi}$,

$$\beta_f = f(-\epsilon/2 + 2v + \sqrt{v}\,f) = f(-\epsilon/3 + \sqrt{\epsilon/12}\,f)\ , \tag{3.127}$$

which obviously has the IR-stable fixed point $f^* = 2\sqrt{\epsilon/3}$. The only really novel renormalization concerns the vertex function $\Gamma_{\bar\phi\bar\varphi\psi}$, yielding

$$\zeta_\rho - \zeta_D = -\epsilon/2 - 2v + \sqrt{v}\,(g + h + f)\ . \tag{3.128}$$

After using $\zeta_{\mu'} - \zeta_{\bar\mu} = \sqrt{v}(h - f - \bar f)$, this leads to

$$\begin{aligned} \beta_{\bar f} &= \bar f[-\epsilon/2 - 2v + \sqrt{v}\,(g + 2h - \bar f)] = \\ &= \bar f(\epsilon/3 - \sqrt{\epsilon/12}\,\bar f)\ . \end{aligned} \tag{3.129}$$

Comparing with Eq. (3.127), we see that the non-trivial fixed point $\bar f^* = 2\sqrt{\epsilon/3}$ is *unstable*, whereas $\bar f^* = 0$ is stable for $d < 4$. Consequently, the three-species vertex $\Gamma_{\bar\phi\bar\varphi\psi}$ vanishes asymptotically, i.e., becomes irrelevant, which implies

$$\bar\phi = (\zeta^*_{\bar\mu} - \zeta^*_D)/\zeta^*_\tau = 1 + O(\epsilon^2)\ , \tag{3.130}$$

identical with the one-loop values of the crossover exponents ϕ and ϕ'. Coupling to an additional hierarchy level therefore does *not* introduce a novel crossover exponent in the multicritical regime, at least to $O(\epsilon)$. We suspect that this is actually true to higher orders in $\epsilon = 4 - d$ and for higher levels $i > 3$ as well.

On the other hand, below the critical dimension $d_c = 4$ the density exponents β_i are affected by the fluctuation corrections to the scaling functions, and are not simply determined by a scaling relation like Eq. (2.37) [23]. In fact, were such a renormalization contribution from the scaling function absent, we would arrive at $\beta_i = 1/2^{i-1} - \epsilon/6$ to one-loop order, with the $O(\epsilon)$ correction *independent* of the level index i. This would predict that near four dimensions, i.e., for any $0 < \epsilon \ll 1$, β_i should become negative for sufficiently large i. The correct result (3.99) for the second hierarchy level, however, shows that the $O(\epsilon)$ correction is actually smaller than for the first level. Presumably, on each successive level the $O(\epsilon)$ corrections are further reduced, such that all the

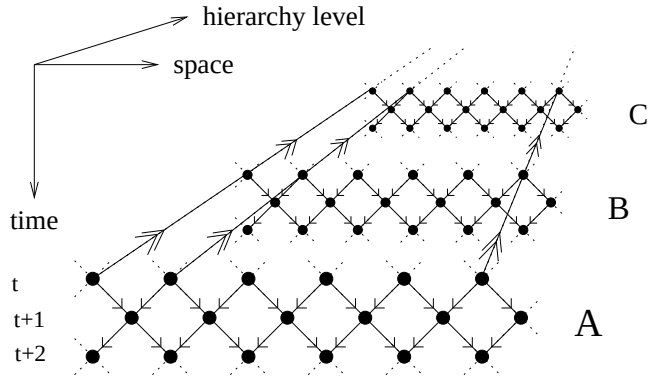

FIG. 11. Schematical illustration of a coupled hierarchy of three directed bond percolation processes in 1+1 dimensions. Activity percolates along the direction of time through bonds (simple arrows) which are open with probability p. The three subsystems are coupled by instantaneous transfer of activity (double arrows) to the corresponding site of the next subsystem.

density exponents remain positive. A detailed computation of β_3, which requires an explicit study of the active phase, already becomes a rather tedious affair, and we leave our discussion of higher hierarchy levels with this speculation.

IV. NUMERICAL RESULTS

In order to support our field-theoretical results, we study a unidirectionally coupled hierarchy of DP models using Monte-Carlo simulations. There is a large variety of DP lattice models that can be used for this purpose. One of the simplest and most efficient realizations is *directed bond percolation* on a tilted square lattice [27]. In this model, neighboring sites are connected by directed bonds which are open with probability p and closed otherwise. Activity percolates through open bonds along a given direction which is usually interpreted as the direction of time. Labelling different rows of sites by a discrete time variable t, directed bond percolation may be equivalently defined as a stochastic cellular automaton with parallel update rules mapping the system's configuration at time t probabilistically onto a set of new configurations at time $t+1$. In one spatial dimension, directed bond percolation is just a special case of the Domany–Kinzel cellular automaton [28] which is known to be one of the most efficient realizations of DP on a computer. Another advantage of using directed bond percolation is the availability of very precise estimates for the critical percolation threshold $p_c(d)$ in $d \leq 2$ spatial dimensions. Currently the best estimates are $p_c(1) = 0.644\,700\,15(5)$ [29] for $d = 1$ and $p_c(2) = 0.287\,338(6)$ [30] for $d = 2$, respectively. To our knowledge, the percolation threshold for $(3+1)$-dimensional directed bond percolation has not been estimated before. Using standard methods we find the value $p_c(3) = 0.13235(20)$.

Coupled DP may be realized on a computer by simultaneously evolving several directed bond percolation models which are coupled without feedback according to the principles outlined in the Introduction (see Fig. 11). For simplicity, we work in the limit of infinite coupling strength $\mu = \infty$, i.e., active sites in one of the subsystems instantaneously turn the corresponding sites of the next subsystem into the active state. Alternatively, we could also apply a finite coupling strength (probabilistic transfer of activity to the next subsystem), or explicit particle transmutation $A \to B, B \to C, \ldots$. Although these variants are expected to have the same critical properties, their initial crossover times into the scaling regime are typically longer. Therefore we restrict the numerical analysis to the case of infinite coupling strength.

In principle it would be possible to simulate arbitrarily many hierarchy levels. However, in order to reach the scaling regime, the particle densities have to be low enough. It turns out that already at the fourth level the particle density is rather high, which makes it extremely difficult to determine critical exponents. For this reason our numerical simulations are restricted to three hierarchy levels.

A. Numerical estimation of the critical exponents

In order to estimate the critical exponents of coupled DP, we employ two standard numerical methods for systems with phase transitions into absorbing states. On the one hand, we use steady-state simulations in the active phase in order to directly determine the exponents β_k. On the other hand, dynamical simulations [31] at the multicritical point render a set of dynamic exponents which in turn determine the exponents $\nu_{\perp,k}$ and $\nu_{\parallel,k}$.

a. Steady state simulations in the active phase. On the multicritical line the stationary particle densities n_k are expected to scale as $n_k \sim (p - p_c)^{\beta_k}$. By measuring n_k in a sufficiently large system, it is therefore possible to directly estimate the exponents β_k. The accuracy of the results depends on the accessible range of $\Delta p = p - p_c$ in the simulation. In $d = 1$ spatial dimension the minimal value of $p - p_c$ is predominantly limited by the equilibration time $T_{\rm equ}$ which has to be larger than the temporal correlation length $\xi_{\parallel,k} \sim (p - p_c)^{-\nu_{\parallel,k}}$, whereas in $d \geq 2$ dimensions the main limitation is the system size $N_{\rm max}$, which has to be larger than $\xi^d_{\perp,k} \sim (p - p_c)^{-d\nu_{\perp,k}}$ (see Table I). The measurements for $d = 1$ are shown in Fig. 12a. From the slopes of the lines averaged over one decade we estimate the exponents β_i, whose values are listed in Table I.

b. Dynamical simulations at the multicritical point. The most precise estimates for the critical exponents of systems with phase transitions into absorbing states are usually obtained by dynamical simulations [31]. Starting from an initial state with a single particle (active seed), the system evolves at the critical point and generates a spatio-temporal cluster of active sites whose size and lifetime is finite. Survival probability, mass, and mean

	$d=1$	$d=2$	$d=3$	$d=4-\epsilon$
$\Delta p_{\min}$	0.0004	0.0008	0.0016	
$N_{\max}$	4000	100^2	35^3	
$T_{\rm equ}$	10^5	10^4	10^3	
β_1	0.280(5)	0.57(2)	0.80(4)	$1-\epsilon/6+O(\epsilon^2)$
β_2	0.132(15)	0.32(3)	0.40(3)	$1/2-\epsilon/8+O(\epsilon^2)$
β_3	0.045(10)	0.15(3)	0.17(2)	$1/4-O(\epsilon)$
$\beta_{\rm DP}$	0.2765	0.584	0.81	

TABLE I. Steady-state simulation results.

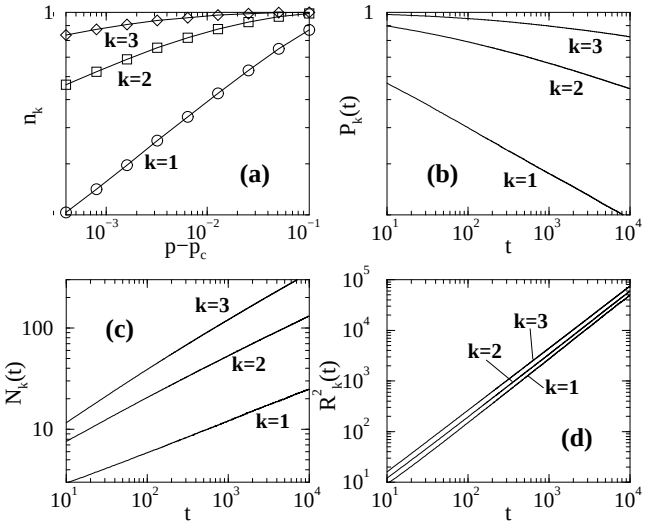

FIG. 12. Monte Carlo simulations of coupled DP in $1+1$ dimensions. a): Steady-state simulations in the active phase. b)-d): Dynamical simulations at criticality. Time is measured in Monte Carlo steps.

	$d=1$	$d=2$	$d=3$	$d=4-\epsilon$
t_{max}	10^4	10^3	300	
δ_1	0.157(4)	0.46(2)	0.73(5)	$1-\epsilon/4+O(\epsilon^2)$
δ_2	0.075(10)	0.26(3)	0.35(5)	$1/2-\epsilon/6+O(\epsilon^2)$
δ_3	0.03(1)	0.13(3)	0.15(3)	$1/4-O(\epsilon)$
η_1	0.312(6)	0.20(2)	0.10(3)	$\epsilon/12+O(\epsilon^2)$
η_2	0.39(2)	0.39(3)	0.43(5)	$1/2+O(\epsilon^2)$
η_3	0.47(2)	0.56(4)	0.75(10)	$3/4-O(\epsilon)$
$2/z_1$	1.26(1)	1.10(2)	1.03(2)	
$2/z_2$	1.25(3)	1.12(3)	1.04(2)	$1+\epsilon/24+O(\epsilon^2)$
$2/z_3$	1.23(3)	1.10(3)	1.03(2)	

TABLE II. Dynamical simulation results.

square spreading of the cluster vary algebraically with certain dynamical exponents which in turn are related to the exponents β, $\nu_\perp$, and $\nu_\parallel$. In order to apply this technique to coupled DP, we prepare an initial state with a single A particle at the origin and perform the simulation at the multicritical point. The properties of the resulting cluster are analyzed separately for each particle species, i.e., we measure the survival probability $P_k(t)$, the number of k-particles (cluster mass) $N_k(t)$, and the mean-square spreading from the origin $R_k^2(t)$ averaged over all runs that survived at level k up to time t. At the multicritical point, these quantities are expected to scale as

$$P_k(t) \sim t^{\delta_k} \ , \quad N_k(t) \sim t^{\eta_k} \ , \quad R_k^2(t) \sim t^{2/z_k} \ , \qquad (4.1)$$

where $\delta_k = \beta_k/\nu_{\parallel,k}$ and $z_k = \nu_{\parallel,k}/\nu_{\perp,k}$. Here, η_k is the so-called critical initial slip exponent [32,21] which will be discussed below (not to be confused with the static correlation function Fisher exponent η).

The temporal variation of the quantities (4.1) measured in a three-level coupled directed bond percolation model in $1+1$ dimensions is shown in Fig. 12b-d. Similar simulations were performed in two and three spatial dimensions. From the slopes of the lines averaged over two decades we estimate the critical exponents δ_k, η_k and z_k, which are summarized in Table II. Notice that z_1, z_2, and z_3 assume the same values within the numerical error. Inserting the previous estimates for β_k, we can compute the scaling exponents $\nu_{\parallel,k} = \beta_k/\delta_k$ and $\nu_{\perp,k} = \nu_{\parallel,k}/z_k$ separately for each level k in the hierarchy (see Table III). Within numerical error they coincide with the DP exponents $\nu_\perp$, $\nu_\parallel$, and z, as predicted by the field-theoretical RG calculation.

c. General problems. The extensive simulations reveal an unexpected deviation from ideal scaling at higher levels. As can be seen in Fig. 12, the lines for $k>1$ are in fact not perfectly straight but slightly bent. In order to illustrate these deviations, we determined the local slope of the survival probabilities

$$\delta_k(t) = \frac{\log_{10} P_k(2t) - \log_{10} P_k(t)}{\log_{10} 2} \qquad (4.2)$$

and similarly $\eta_k(t)$ in a $(1+1)$-dimensional system. After sufficiently long times, these quantities should become

	$d=1$	$d=2$	$d=3$	$d=4-\epsilon$
$\nu_{\perp,1}$	1.12(4)	0.70(4)	0.57(4)	
$\nu_{\perp,2}$	1.11(15)	0.69(15)	0.59(8)	$1/2+\epsilon/16+O(\epsilon^2)$
$\nu_{\perp,3}$	0.95(25)	0.65(15)	0.62(9)	
$\nu_{\perp,\mathrm{DP}}$	1.0968	0.734	0.57	
$\nu_{\parallel,1}$	1.78(6)	1.24(6)	1.10(8)	
$\nu_{\parallel,2}$	1.76(25)	1.23(17)	1.14(15)	$1+\epsilon/12+O(\epsilon^2)$
$\nu_{\parallel,3}$	1.50(40)	1.15(30)	1.21(15)	
$\nu_{\parallel,\mathrm{DP}}$	1.7338	1.295	1.09	

TABLE III. Derived critical exponents.

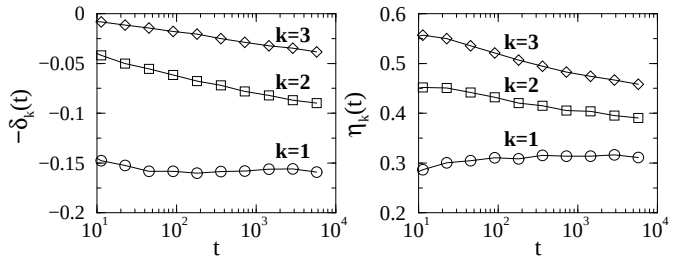

FIG. 13. Local slopes of the lines in Fig. 12b-c. The slow drift of the slopes at higher levels indicates that the scaling regime is not yet reached in the present simulations. (Time is measured in Monte Carlo steps.)

constant and equal to the exponents δ_k and η_k, respectively. As expected, the lowest level reaches the scaling regime after a short time (see Fig. 13). At higher levels, however, there is a considerable drift of the local slope that extends over the entire temporal evolution. Similar drifts can be observed in all other quantities which involve the density exponents $\beta_2, \beta_3, \ldots$. The deviations indicate that the scaling regime, especially at the third level, has not yet been reached. By estimating the critical exponents at higher levels, we therefore encounter considerable systematical errors which may even exceed the statistical error margins. A careful numerical analysis shows that the drift in the local slopes is neither related to finite-size effects nor to deviations from criticality. At present the origin of these deviations from ideal scaling is not yet entirely clear. It might perhaps be a signature of the IR-divergent diagram (c) of Fig. 9 (see Sect. III F). As mentioned above, these graphs are connected with the appearance of additional powers of the *relevant* coupling μ, and we suspect that this drift in the scaling exponents signals that our first-order perturbation theory with respect to the transmutation rate becomes ultimately insufficient, and some appropriate resummation of the expansion in μ would in fact be required.

Furthermore, we remark that in a simulation based of course on a finite number of particles, ultimately one would expect a crossover to the *decoupled* situation, namely when the A species, whose density decays *faster* at the multicritical point, has already died out. It might well be possible that in a fluctuation-dominated regime this effect sets in much earlier, provided there emerge large regions which have already become depleted of the A particles. Thus, one explanation of the drifts visible in Fig. 13 could be that this crossover region to the asymptotic decoupled regime has already been reached. The universal exponents predicted by the field theory would then apply only to an intermediate scaling regime. We note that the field theory calculation, being based on a continuum description of coarse-grained particle densities, cannot easily account for this finiteness of the particle number.

In the case of coupled annihilation processes (see Sec. VI), where similar deviations occur, the intermediate scaling regime can be clearly identified in numerical simulations. In particular it is observed that the size of the scaling regime grows as the coupling strength decreases. We have also performed simulations of coupled DP with reduced coupling strength (probabilistic transfer of activity to the next level). Unfortunately, the initial crossover into the intermediate scaling regime grows rapidly as the coupling strength is reduced which makes it impossible to identify the boundaries of the intermediate scaling regime.

B. Critical initial slip

When a DP process starts from random initial conditions at very low density, the particles are initially separated by empty intervals of a certain typical size. During the temporal evolution these particles generate individual clusters which are initially separated. Therefore the average particle density first *increases* as $n(t) \sim t^{\eta}$ — a phenomenon which is referred to as the *critical initial slip* of non-equilibrium systems [32]. Later, when the growing clusters begin to interact with each other, the DP process crosses over to the usual decay $n(t) \sim t^{-\beta/\nu_\parallel}$. Dynamical simulations starting from a single particle represent the extreme case where the critical initial slip extends over the entire temporal evolution.

In ordinary DP, the critical initial slip exponent η is related to the other bulk exponents through the hyperscaling relation $2\delta + \eta = d/z$ [31,21]. In the case of coupled DP we would therefore naively expect that the critical initial slip exponents η_k are related to the other exponents by $2\delta_k + \eta_k = d/z$. However, the numerical estimates in Tables II and III do *not* satisfy this scaling relation at higher levels $k > 1$. Instead they seem to fulfil the *generalized hyperscaling relation* introduced in Ref. [33] in the context of systems with many absorbing states,

$$\delta_{\mathrm{DP}} + \delta_k + \eta_k = d/z_k \ . \tag{4.3}$$

Here δ_{DP} denotes the exponent $\beta/\nu_\parallel$ of ordinary directed percolation. In fact, inserting the estimates of δ_k and z_k for $d = 1$, Eq. (4.3) predicts the values $\eta_1 = 0.314(4)$, $\eta_2 = 0.398(10)$, and $\eta_3 = 0.443(20)$, which are in fair agreement with the estimations in Table III.

In fact, the above scaling relation (4.3) may be derived fairly simply, starting from an appropriate scaling form

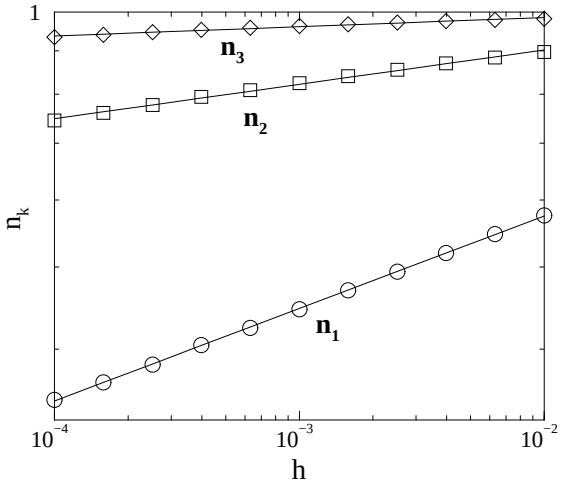

FIG. 14. Susceptibility of multicritical coupled DP to an external field. The figure shows the stationary particle densities n_k versus the rate h for spontaneous particle creation.

for the two point correlation function. If we initiate the cluster starting from a single localized seed, then the density of B particles at a later time will have the following form:

$$n_2(x,t) \sim |\tau|^{2\beta_1} \hat{f}_1 \left(\frac{\mu/D}{|\tau|^{\phi}}, \frac{x}{|\tau|^{-\nu_\perp}}, \frac{Dt}{|\tau|^{-\nu_\parallel}} \right) . \qquad (4.4)$$

Note that, even though this is a scaling form for the *density*, it has the structure of a two point correlation function. Roughly speaking, the prefactors in Eq. (4.4) may be interpreted as follows: one factor of $|\tau|^{\beta_1}$ comes from the probability that the cluster is still alive at time t, whilst the second factor comes from the probability that the point (x,t) is a member of that cluster. At criticality we find, by integrating (4.4) over space

$$t^{\eta_2} \sim t^{(d\nu_\perp - 2\beta_1)/\nu_\parallel} \hat{f} \left(\frac{\mu/D}{(Dt)^{-\phi/\nu_\parallel}} \right) , \qquad (4.5)$$

where we have also used one of the definitions from Eq. (4.1). Assuming that the scaling function $\hat{f}$ in the multicritical regime behaves in the same way as in Sec. III E, we then end up with the scaling relation (4.3) for the second hierarchy level. The extension to higher levels works in an exactly similar manner.

C. Susceptibility to an external field

Coupled DP may be subjected to an external field $h > 0$ by adding a term $h \int d^dx \int dt\, \bar{a}$ to the action (3.1). In the particle interpretation, the field corresponds to a spontaneous creation of A particles at rate h during the temporal evolution. This means that all subsystems approach a fluctuating steady state, irrespective of the value of p. We are particularly interested in the response of n_k to the external field at the multicritical point. For ordinary DP it is known that $n_1 \sim h^\gamma$, where $\gamma = \beta/(d\nu_\perp + \nu_\parallel - \beta)$ is the susceptibility exponent. For coupled DP we can derive a similar relation, starting from the scaling form for the (steady-state) density

$$n_2 \sim |\tau|^{\beta_1} \hat{g}_1 \left(\frac{\mu/D}{|\tau|^{\phi}}, \frac{|\tau|}{h^{1/\Delta}} \right) , \qquad (4.6)$$

where the DP exponent Δ can be shown to equal $\Delta = d\nu_\perp + \nu_\parallel - \beta_1$. In the limit $|\tau| \to 0$, we thus have

$$n_2 \sim h^{\beta_1/\Delta} \hat{g} \left(\frac{\mu/D}{h^{\phi/\Delta}} \right) . \qquad (4.7)$$

Hence, using the results of Sec. III E and generalizing to the k-th level of the hierarchy, we have

$$n_k \sim h^{\gamma_k} , \qquad \gamma_k = \frac{\beta_k}{d\nu_\perp + \nu_{||} - \beta_1} . \qquad (4.8)$$

In order to verify this scaling relation, we repeat the steady-state simulation at the multicritical point in presence of spontaneous creation of A particles. The results in $1+1$ dimension are shown in Fig. 14. From the slopes of the lines we estimate the susceptibility exponents

$$\gamma_1 = 0.109(2) \ , \ \gamma_2 = 0.045(4) \ , \ \gamma_3 = 0.014(2) \ . \qquad (4.9)$$

On the other hand, the above scaling relation yields the values $\gamma_1 = 0.107(2)$, $\gamma_2 = 0.051(6)$, and $\gamma_3 = 0.018(5)$, which are in fair agreement with the simulation results.

D. Crossover phenomena near the multicritical point

Numerical simulations near the critical point reproduce the crossover scenario predicted by the mean-field approximation. As an example, we consider the two crossovers along the dashed arrows A and A/B in the mean-field phase diagram of Fig. 1. To this end, we simulate a two-level system in one spatial dimension. The percolation probability p_1 of level A is always at the critical point, whereas level B is simulated slightly below and above criticality ($p_2 = p_c \pm 0.05$). The numerical results are shown in Fig. 15. As expected, for $p_2 < p_c$ the density of B particles first decays like $n_2(t) \sim t^{-\beta_2/\nu_\parallel}$ and then crosses over to a dynamical state where the B particles become "slaved" to the A particles, such that $n_2(t) \sim n_1(t) \sim t^{-\beta_1/\nu_\parallel}$. On the other hand, for $p_2 > p_c$ the B subsystem crosses over into a state with a constant density where the B particles become independent of the A particles. Thus the crossover effects are in qualitative agreement with the mean-field and RG predictions of Secs. II and III H.

V. APPLICATIONS

The most natural applications of coupled DP are to growth processes in which the layers at different heights

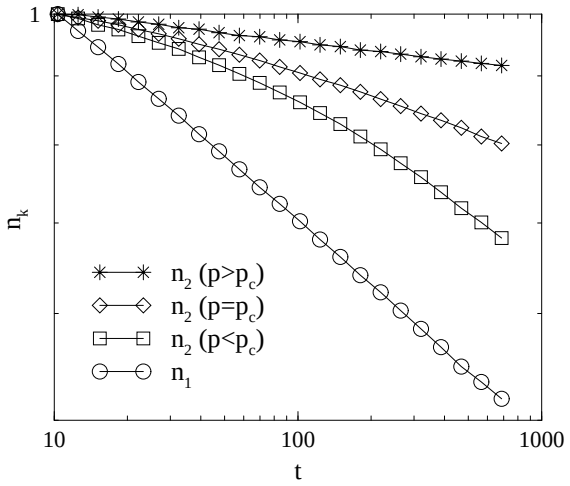

FIG. 15. Crossover effects near the multicritical point. The figure shows the particle densities n_k vs time in a two-level system starting from a fully occupied lattice, normalized at $t = 10$. Level A ($k = 1$) is always critical, while level B ($k = 2$) is either evolving in the active, critical, or inactive regime. Initially the decay of B particles is the same in all cases. Later the system crosses over to a different behavior where the B particles become independent or slaved to the A particles, respectively. (Time is measured in Monte Carlo steps.)

represent different subsystems in the hierarchy. The dynamical rules for adsorption and desorption in these models have to be implemented in such a way that neighboring layers are effectively coupled in one direction without feedback. The phase transition then emerges as a roughening transition from a smooth phase to a rough phase. The known examples include so-called polynuclear growth models (PNG) [34], a special class of solid-on-solid (SOS) models [35], and certain models for fungal growth [36]. Another interesting realization of coupled DP is the spreading of activity next to the "light cone" in stochastic cellular automaton models with parallel update rules.

A. Roughening transitions in SOS models

Coupled DP was first identified in a particular SOS model [35] which exhibits a roughening transition even in one spatial dimension. The active phase of coupled DP corresponds to a smooth phase where the interface is pinned to a spontaneously selected layer. On the other hand, the inactive phase of coupled DP corresponds to a roughening interface which propagates at finite velocity.

The unrestricted version of the SOS model is defined on a one-dimensional lattice of N sites, $i = 1 \dots N$, with associated height variables h_i, which may take values $0, 1 \dots \infty$. The dynamical rules are defined through the following algorithm: At each update a site i is chosen at random. Then an atom is adsorbed,

$$h_i \to h_i + 1 \text{ with probability } q \ , \tag{5.1}$$

or desorbed from the edge of an island (plateau),

$$h_i \to \min(h_i, h_{i+1}) \text{ with probability } (1-q)/2 \ , \tag{5.2}$$
$$h_i \to \min(h_i, h_{i-1}) \text{ with probability } (1-q)/2 \ . \tag{5.3}$$

When the growth rate q is low, the desorption processes (5.2) and (5.3) dominate. If all the heights are initially set to the same value h_0, this layer will remain the bottom layer of the interface. Small islands will grow on top of the bottom layer, but will quickly be eliminated by desorption at the island edges. Thus, the interface is effectively anchored to its bottom layer, and the growth velocity, defined as the rate of increase of the minimum height of the interface, is zero in the thermodynamic limit. As q is increased, the size of islands created on top of the lowest layer increases. Above q_c, the critical value of q, the islands merge and new layers are formed at a finite rate, giving rise to a non-zero interface velocity in the thermodynamic limit.

The key feature of this model is that atoms may desorb only at the *edges* of plateaus, i.e., at sites which have at least one neighbor at a lower height. In experiments this would correspond to a system where the binding energy in completed layers is much larger than at the edges of plateaus. Furthermore, the dynamical processes at a given layer are independent of the processes at higher layers. In particular, the temporal evolution at the bottom layer is decoupled from all other processes at higher layers. In fact, one can show that the dynamics of the bottom layer can be mapped onto a one-dimensional contact process which is known to belong to the DP universality class [35]. Identifying blank sites at the bottom layer as A particles, the adsorption process (5.1) may be interpreted as the annihilation of A particles, while the desorption process (5.2)–(5.3) corresponds to A particle production. Similarly, the dynamical processes at the following layers may be associated with the particle species $B, C, D, \dots$.

It is important to note that the state of a site in coupled DP is characterized by presence or absence of various particle species, while sites of a growth model are associated with a single quantity, namely the height h_i. To connect the two descriptions, we have to assume that the coupling constant μ is infinite such that particles at level k instantaneously create particles at level $k+1$. In this case the state of a site in coupled DP is fully characterized by the index of the lowest active level in the hierarchy, which then corresponds to the height of the interface in the growth model. Therefore, the order parameters $n_A, n_B, n_C, \dots = n_1, n_2, n_3 \dots$ are defined by

$$n_k = \frac{1}{N} \sum_i \sum_{h=h_0}^{h_0+k-1} \delta_{h_i,h} \ , \tag{5.4}$$

that is, n_k is the density of sites whose heights are *less* than $h_0 + k$, where h_0 denotes the height of the bottom layer. By definition, the densities obey the inequality $n_k \le n_{k+1}$.

The above growth model is invariant under global shifts of the heights $h_i \to h_i + a$. This symmetry is spontaneously broken in the (coupled DP) active phase where the system selects a particular reference height as the bottom layer. In the (coupled DP) inactive phase, however, the interface becomes rough and propagates at finite velocity, i.e., active DP processes subsequently enter the absorbing state. The growth velocity v is inversely proportional to the average survival time of the lowest-lying DP process, hence $v \sim (q - q_c)^{\nu_{||}}$. Numerical simulations confirm that the critical behavior of the first few layers in the growth model is indeed the same as in coupled DP. In particular, the exponents β_k for the density of sites at the first few layers are in agreement with the numerical estimates in the present work.

Alternatively, one may study the same model with the additional restriction $|h_i - h_{i\pm1}| \leq 1$. In that case the layers are no longer coupled without feedback. For example, if a site with height $h_i = 1$ has neighbors at heights $h_{i-1} = 0$ and $h_{i+1} = 2$, the atom at site i cannot desorb from the surface. Using the language of coupled DP, this means that the presence of C particles prevents the A particles from producing offspring. Surprisingly, the numerical estimates of the exponents β_k indicate that the critical behavior of the system is still that of coupled DP. Thus it seems that certain realizations of "inhibiting" feedback from higher levels to lower ones do not destroy the universal properties of coupled DP. Rather, the essential precondition for coupled DP seems to be the existence of a hierarchy of absorbing subspaces, i.e., inactive levels must not be activated by higher levels.

B. Polynuclear growth models

In PNG models [34] a similar scenario arises, but in this case the coupled DP behavior occurs at the highest levels of the interface. As in the previous case, the PNG models may be defined on a square lattice with associated height variables h_i. The key feature of these models is the use of *parallel updates* which gives rise to a maximum velocity of the interface. One of the most popular PNG models is defined through the following dynamical rules. In the first half time step atoms "nucleate" stochastically at the surface by

$$h_i\left(t+\frac{1}{2}\right) = \begin{cases} h_i(t)+1\ , & \text{with probability } p \\ h_i(t)\ , & \text{with probability } 1-p\ . \end{cases} \tag{5.5}$$

In the second half time step the islands grow deterministically until they coalesce

$$h_i(t+1) = \max_j \left[h_i\left(t+\frac{1}{2}\right), h_j\left(t+\frac{1}{2}\right)\right]\ , \tag{5.6}$$

where j runs over the nearest neighbors of site i. Starting from a flat interface $h_i(0) = 0$, the sites at maximal height $h_i(t) = t$ may be considered as active sites of a DP process. Obviously Eq. (5.5) turns active into inactive sites with probability $1 - p$, while offspring production is realized by the process (5.6). Therefore, if p is large enough, the interface is smooth and propagates with velocity 1. Below a critical threshold, however, the density of active sites at the maximal height $h_i(t) = t$ vanishes, and the growth velocity is smaller than 1. Identifying the sites with $h_i = t$ as A particles, those with $h_i \geq t-1$ as B particles etc., the dynamical processes resemble the rules of coupled DP. The corresponding order parameters are defined by

$$n_k = \frac{1}{N} \sum_i \sum_{h=0}^{k-1} \delta_{h_i, t-h}\ . \tag{5.7}$$

Thus PNG models may be interpreted as a realization of coupled DP in a *co-moving* frame. An exact mapping relating PNG models and the previously discussed SOS models (where coupled DP resides in a fixed frame next to the bottom layer) was proposed in Ref. [35]. It should be emphasized that the existence of a roughening transition in PNG models requires the use of parallel updates. If random-sequential updates are used, the transition is lost, and the interface is always rough since then there is no maximum velocity.

C. Models for fungal growth

Recently, López and Jensen [36] introduced a class of models for the growth of colonial organisms, such as fungi and bacteria. The models are motivated by recent experiments [37] with the yeast *Pichia membranaefaciens* on solidified agarose film. Depending on the concentration of polluting metabolites, different front morphologies were observed. The aim of the models is to explain these morphological transitions on a qualitative level.

The model for fungal growth is defined on a triangular $(1 + 1)$-dimensional lattice whose sites are either occupied or vacant. Growth of the colony occurs because of the division of individual cells, i.e., only nearest neighbors of occupied sites can become occupied. T he model evolves by *parallel* updates. To mimic realistic cells, it is assumed that cell division is less likely in young cells. To this end, the simulation keeps track of the age $a_j(t)$ of occupied sites. The probability $P_i(t)$ for a vacant site i to become occupied in the next time step depends on the total age $A_i(t) = \sum_{\langle i,j\rangle} a_j(t)$ of the occupied nearest neighbors of site i. Using the functional dependence $P_i(t) = \tanh[\theta A_i(t)]$, a roughening transition was observed at $\theta_c = 0.183(3)$. Investigating clusters of sites growing at maximal velocity, some of the critical properties at the transition could be related to DP [36]. It was argued that this roughening transition could be the essential mechanism behind the morphological transitions observed in experiments.

Clearly the above fungal model and the PNG models are very similar in character. They both work with parallel updates and exhibit a roughening transition which is

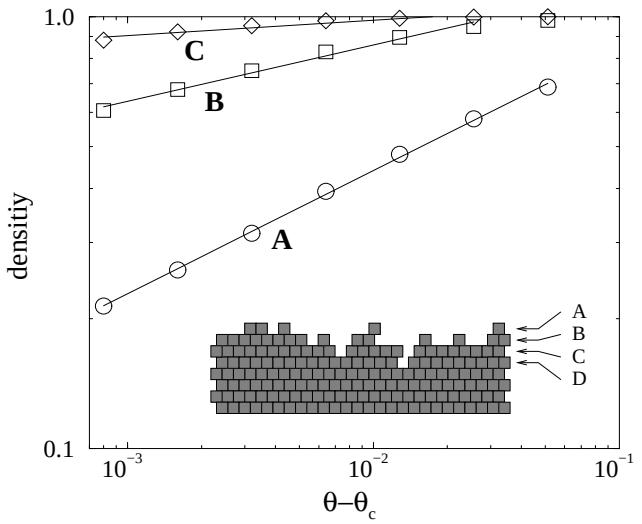

FIG. 16. Coupled DP in a model for fungal growth. The graph shows the density of the first three levels propagating at maximal velocity as a function of $\theta - \theta_c$ in the smooth phase. Power-law fits are used to estimate the exponents β_k (see text). The inset shows a typical configuration of the growing front near criticality.

related to DP. Here we will present numerical evidence to show that the fungal growth model is actually a realization of coupled DP, in spite of complicated details such as the age-dependent rates for cell division and interface overhangs. The order parameters n_k may be defined as

$$n_k = \frac{1}{N} \sum_i N_i(t)\, \delta_{y_i, t-k+1} \ , \tag{5.8}$$

where $N_i(t) = 0, 1$ denotes the occupation number of site i, and y_i is the height coordinate of the i-th site. We have numerically measured the densities n_1, n_2, and n_3 near criticality in the smooth phase (see Fig. 16). Our estimates $\beta_1 = 0.28(2)$, $\beta_2 = 0.13(2)$, $\beta_3 = 0.04(2)$ are in agreement with the numerical results of section IV.

As in the PNG models, the existence of a roughening transition in the model for fungal growth requires the use of parallel updates. For random sequential updates there is no such transition and the interfaces are always rough. However, random sequential updates seem to be a more appropriate description of the experiments in Ref. [37], since realistic cells do not divide synchronously. Therefore it is still unclear to what extent the roughening transition of the model in Ref. [36] is related to morphological transitions in realistic fungal growth.

D. Critical behavior near the light cone in spreading processes with parallel dynamics

Let us finally consider a directed bond percolation process on a tilted square lattice in $d+1$ dimensions, which may be understood as a stochastic cellular automaton evolving by parallel updates [28]. Starting from a single active seed such a cellular automaton generates a cluster of active sites. For maximal percolation probability $p = 1$ this cluster is compact and has the shape of a pyramid. This means that all sites within the *light cone* (the surface of the pyramid) are activated.

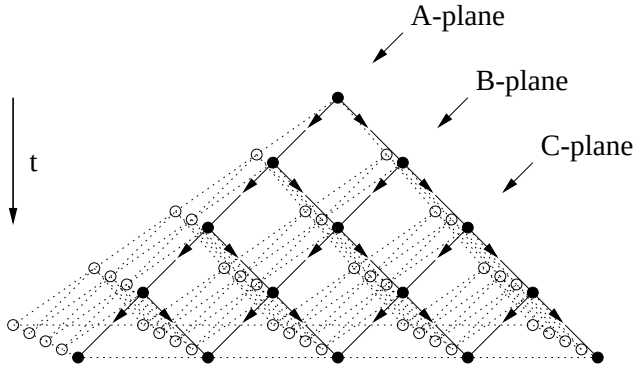

FIG. 17. Realization of a unidirectionally coupled hierarchy of (1 + 1)-dimensional DP processes in a (2 + 1)-dimensional directed bond percolation process with parallel updates. The figure shows the "light cone" starting from a single site. The subsystems A,B,C,... correspond to tilted planes as indicated by the arrows.

Apart from the usual phase transition, DP models with parallel updates in $d \geq 2$ spatial dimensions exhibit a *second* transition, where the clusters detach from their light cone. In the case of (2 + 1)-dimensional directed bond percolation this transition takes place at $p = p_s \simeq 0.6447 > p_c$. As illustrated in Fig. 17, the dynamical processes near the light cone constitute a unidirectionally coupled hierarchy of DP processes in $d-1$ spatial dimensions. The lowest hierarchy level A corresponds to the sites in the light cone. Clearly these sites are decoupled from the interior of the pyramid. The following hierarchy levels B,C,... correspond to parallel planes as indicated in Fig. 17. Since activity can only percolate forward in time, these planes are coupled in only one direction without feedback. The dynamical processes within each subsystem are precisely those of a directed bond percolation process on a tilted square lattice in $d-1$ spatial dimensions. Therefore, the numerical value of p_s in d spatial dimensions coincides with the usual transition point p_c in $d-1$ dimensions. This explains the numerical value $p_s \simeq 0.6447$.

VI. COUPLED ANNIHILATION REACTIONS

We finally return to the question of whether new dynamic universality classes can be constructed by the unidirectional coupling of known non-equilibrium processes. We have seen that in the case of *linearly* coupled directed percolation, the ensuing hierarchical structure leads to the emergence of multicritical behavior at a special point in control parameter space, described by the novel density exponents β_i and α_i. Similarly, we expect identical qualitative features for the closely related problem of lin-

early coupled dynamic (isotropic) percolation processes (albeit there one of the non-linear vertices is non-local in time [14]). This is to be contrasted with the very general *quadratically* coupled multi-color DP processes studied recently by Janssen, where ordinary DP critical behavior is found [15].

The simplest non-trivial case, however, would be to consider a stochastic process which is generically scale-invariant, i.e., where no tuning to a special critical point is required. An example of such a system is provided by the simple diffusion-limited two-particle annihilation reaction [7,8]

$$A + A \to \emptyset \quad \text{with rate } \lambda_A \ . \tag{6.1}$$

The corresponding mean-field rate equation for the particle density A reads

$$\frac{\partial n_A(x,t)}{\partial t} = D\nabla^2 n_A(x,t) - 2\lambda_A n_A(x,t)^2 \ , \tag{6.2}$$

which is solved at long times $t \to \infty$ by $n_A(t) \sim t^{-1}$. Power counting shows that this result is expected to be correct for dimensions $d > d_c = 2$.

In low-dimensional systems, however, fluctuations and the emerging particle-anticorrelations become important, and the density decay exponent is reduced. In order to include these fluctuations consistently, one may derive the following field theory from the classical master equation [8],

$$S = \int d^dx \int dt \Big[\hat{a}(\partial_t - D\nabla^2)a - \lambda_A(1-\hat{a}^2)a^2 \Big] \ , \tag{6.3}$$

where we have omitted boundary terms stemming from the initial configuration, as well as terms related to the projection state (see Ref. [8]). When the action (6.3) is expanded about the stationary solution $\hat{a} = 1$, the classical field equation for $a(x,t)$ yields precisely the mean-field rate equation (6.2). The entire field theory (6.3) can also be recast in the form of a Langevin equation for the field $a(x,t)$, although this field is related to the true density field $n_A(x,t)$ in a rather non-trivial way [17,8,38].

The structure of the field theory (6.3) is very simple, as no diagrams can be constructed that would renormalize the free diffusion propagator $(-i\omega + Dq^2)^{-1}$. Furthermore, the entire perturbation series for the annihilation vertices is readily summed via a geometric series, or through solving the ensuing Bethe-Salpeter equation. Hence the scaling behavior of the density is known exactly. The final result is [8]

$$n_A(t) \sim \begin{cases} t^{-d/2} & \text{for } d < 2 \ , \\ t^{-1} \ln t & \text{for } d = d_c = 2 \ , \\ t^{-1} & \text{for } d > 2 \ . \end{cases} \tag{6.4}$$

Let us now consider a hierarchy of such annihilation processes,

$$B + B \to \emptyset \quad \text{with rate } \lambda_B \ , \tag{6.5}$$

etc., unidirectionally coupled via the branching reaction

$$A \to A + B \quad \text{with rate } \sigma_{AB} \ . \tag{6.6}$$

The choice of this specific coupling can be motivated as follows. If the A species were not to appear on the right-hand-side of the reaction (6.6), then this would constitute a spontaneous death process for the A particles, immediately leading to an exponential density decay. However, on the lowest hierarchy level, we want to retain all the features of the uncoupled reactions [especially the power-law decay of Eq. (6.4)]. Also, we want to keep the coupling reaction linear in the particle density n_A, as in our earlier analysis of coupled DP. Thus, the reaction (6.6) feeds additional particles into level B, which in mean-field theory is described by the rate equation

$$\frac{\partial n_B(x,t)}{\partial t} = D\nabla^2 n_B(x,t) - 2\lambda_B n_B(x,t)^2 + \sigma_{AB} n_A(x,t) \ . \tag{6.7}$$

Obviously for long times (and consequently for low densities), the B particles are now slaved by the A species, and their density "adiabatically" follows $n_A(t)$,

$$n_B(t) \approx \left(\frac{\sigma_{AB}}{2\lambda_B} n_A(t) \right)^{1/2} \sim t^{-1/2} \ . \tag{6.8}$$

As is to be expected, the branching process (6.6) considerably slows down the decay on level B. Within mean-field theory, a straightforward generalization to higher hierarchy levels leads to $n_i(t) \sim t^{-\alpha_i}$, with $\alpha_i = 1/2^{i-1}$ on level i.

In order to include fluctuation effects, we write down the action corresponding to the coupled reactions (6.1), (6.5), and (6.6), setting $\lambda_A = \lambda_B = \lambda$, and $\sigma_{AB} = \sigma$:

$$S = \int d^dx \int dt \Big[\hat{a}(\partial_t - D\nabla^2)a - \lambda(1-\hat{a}^2)a^2 + \hat{b}(\partial_t - D\nabla^2)b - \lambda(1-\hat{b}^2)b^2 + \sigma(1-\hat{b})\hat{a}a \Big] \ . \tag{6.9}$$

Notice that the A propagator has now acquired a formal mass term σ, as opposed to the B particles, for which we still the have the massless diffusion propagator (again, we have assumed identical diffusion constants D for both species). Of course, once the shifts $\hat{a} = 1 + \bar{a}$ and $\hat{b} = 1 + \bar{b}$ are performed, this mass term disappears (as it should), and on the classical level the mean-field rate equation (6.7) is recovered. It is, however, convenient to work with the unshifted field theory (6.9), as it again has the simple property that there are no (UV-divergent) Feynman diagrams that could lead to a renormalization of either of the propagators. This immediately implies that the "mass" σ is *not* renormalized. Thus, as opposed to the case of coupled DP, there is no new non-trivial scaling field here. If we further assume that there is no non-trivial contribution from the scaling function (i.e. unlike the case of coupled DP), then we may thus just insert the true density decay results (6.4) into the mean-field relation (6.8), in order to obtain the asymptotic decay for

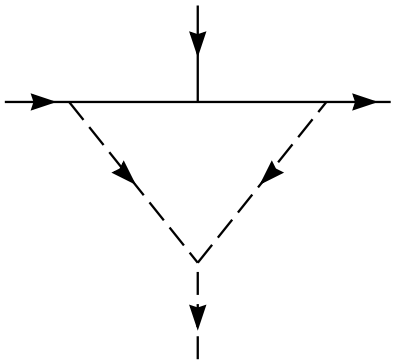

FIG. 18. Coupled annihilation: An IR-divergent diagram contributing to the $aa\bar{a}\bar{b}$ vertex at one-loop order.

the B particles. The result is that the decay exponents are halved on the second hierarchy level. The obvious generalization to level i is therefore

$$n_i(t) \sim \begin{cases} t^{-d/2^i} & \text{for } d < 2 \ , \\ \left(t^{-1} \ln t\right)^{1/2^{i-1}} & \text{for } d = d_c = 2 \ , \\ t^{-1/2^{i-1}} & \text{for } d > 2 \ , \end{cases} \tag{6.10}$$

which, with the above assumption, is an *exact* result at sufficiently long times.

However, in a simulation with *finite* particle numbers, again one would asymptotically expect a crossover to the decoupled scaling regime, namely when there emerge large regions depleted of the A species. Correspondingly, perhaps, one should notice that the coupled annihilation problem is plagued by IR-divergent diagrams which are very similar in nature to the coupled DP case. For example, to one-loop order, the newly generated $aa\bar{a}\bar{b}$ vertex for the massless shifted fields includes a diagram with two massless a and two massless b propagators, as depicted in Fig. 18. This loop integral is infrared-singular whenever $d \leq 6$. One possible interpretation of these additional, apparently non-renormalizable IR singularities, could be that they reflect an eventual *non-universal* crossover to the decoupled regime. Neither, though, can we exclude the possibility that ultimately a very different scaling regime ensues, which would have to be addressed by means of an effective resummation of the expansion with respect to the *relevant* coupling σ.

Numerical simulations of coupled annihilation processes can be performed on the same lattice as in Fig. 11. The stochastic rules have to be chosen in such a way that a particle at site i jumps to one of the neighboring sites with equal probability. When two particles meet at the same place, they annihilate instantaneously. Surprisingly, in the limit of infinite coupling (instantaneous transfer of activity to the next subsystem) the resulting curves in a log-log plot are not straight and do not reproduce the result of Eq. (6.10). A more detailed analysis reveals that the magnitude of these deviations depends strongly on the coupling strength between the subsystems. To this end we replace the instantaneous transfer

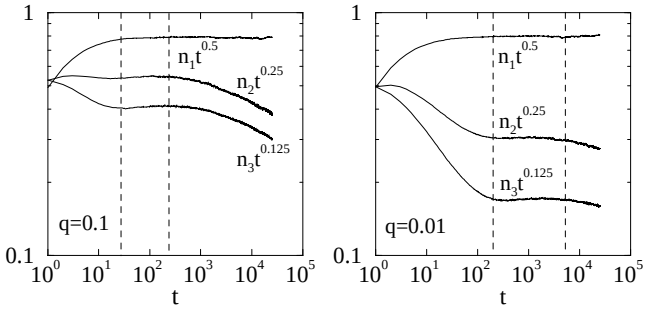

FIG. 19. The coupled annihilation process in $1+1$ dimensions: the graphs show the densities $n_i(t)t^{1/2^i}$ of the first three levels as a function of time for different values of the coupling strength q. The scaling regime is marked by the two dashed lines (see text). Time is measured in Monte Carlo steps.

of activity by a probabilistic rule, i.e., active particles create particles in the next subsystem at the same location with probability q. Clearly, q plays the role of the parameter σ in the field theory. By varying q we observe that the prediction of Eq. (6.10) is only valid in a *limited* scaling regime. As q decreases, the size of the scaling regime grows, as illustrated in Fig. 19. On the other hand, the initial crossover into the scaling regime also grows with q. Similar simulations in $3+1$ dimensions for maximal q suggest that these deviations still persist above the critical dimension although they are much less pronounced in that case. This supports the conjecture that the breakdown of the scaling regime is caused by IR-singular diagrams related to additional powers of σ, which would even invalidate the simple mean-field approach.

Concluding this section, we note that novel critical behavior does not necessarily arise in the unidirectional coupling of stochastic processes. A counterexample is given by the following variant of coupled annihilation, where we replace the reaction (6.6) with

$$A + A \to B + B \quad \text{with rate } \lambda_{AB} \ . \tag{6.11}$$

The ensuing coupled diffusion-limited reaction processes are a special case of the more general system where the back reaction $B + B \to A + A$ is present as well. The full system was studied by field-theoretic means in Ref. [38]. Through an analysis of the coupled Bethe-Salpeter equations for the four non-linear vertices, it was shown in [38] that the A and B reactions asymptotically decouple, and each particle species decays according to Eq. (6.4). The physical reason for this is of course that two particles are required to meet in order for the coupling reaction (6.11) to take place. Thus, this reaction competes with the annihilation process itself, and, in addition, as the daughter B particles appear on the same sites, they have a high probability to annihilate again immediately. This is somewhat related to the robustness of the DP universality class for *quadratically* coupled DP processes [15].

VII. SUMMARY AND DISCUSSION

The simulations presented in the last few sections show good agreement with the predictions of the underlying field theory for a certain range of the parameter τ for coupled DP. Similarly, good agreement is also found for a range of times t for coupled annihilation (or coupled DP at criticality). Nevertheless, deep into the critical region the simulations show a drift in the critical scaling exponents of the second and higher hierarchy levels, perhaps towards their decoupled values. It is not clear, however, if this drift will go all the way towards attaining the decoupled values of these exponents. Furthermore, the drift is more pronounced in the coupled annihilation model where, by decreasing the strength of the inter-species coupling, one can extend the range of the intermediate power-law behavior and delay the onset of the drift.

From the field-theoretical point of view we believe the drift might be due to the increasing effect of the IR-problematic diagrams which were identified both for the coupled DP problem as well as for the coupled annihilation problem. These diagrams contain higher powers of the *relevant* inter-species coupling and thus are suppressed for small values of this coupling. On the other hand, they become more dominant for larger values of the transmutation rate, which, being a relevant operator, increases as one goes deeper into the critical region. This might perhaps render the asymptotic field theory, for large inter-species coupling, non-renormalizable. Note that the simulations for coupled annihilation show that the drift in the value of the exponents for the second and higher hierarchy levels persists even for $d = 3$ which is above the upper critical dimension $d_c = 2$ for the first hierarchy level. This shows that even mean-field theory may not be valid at $d = 3$, consistent with the fact that there exist IR-singular diagrams diverging for any $d \leq 6$. Technically, a resummation of the power expansion with respect to μ or σ would be desirable; unfortunately, a more satisfactory approach to this problem is not yet known.

We propose the following interpretation of this scenario: eventually we expect a *non-universal* crossover into decoupled behavior. This is because in a real system, due to the discreteness of the number of particles, which is always an integer, there are likely to be large regions with no A particles at all, and there the B particles will behave as if they are decoupled from the A species. This is also true for higher hierarchy levels. Thus we have an interesting case in which the field theory predicts correctly the scaling in an *intermediate universal* critical regime, but eventually breaks down deep in the asymptotic limit. There is of course the possibility that one might construct a meaningful field theory for the asymptotic regime which will describe a crossover to a different critical behavior, distinct from both the intermediate regime and the decoupled behavior, but this seems a difficult task and perhaps even an unlikely scenario at this time.

ACKNOWLEDGMENTS

We benefited from discussions with J.L. Cardy, A. Duncan, M.R. Evans, E. Frey, Y. Frishman, H.K. Janssen, M. Moshe, D. Mukamel and A. Schwimmer. We are indebted to an anonymous referee for very helpful comments and suggestions. Y.Y.G. acknowledges support from the US Department of Energy (DOE), grant No. DE-G02-98ER45686. He also thanks the Weizmann institute, where he started working on this problem, and in particular E. Domany and D. Mukamel for their kind hospitality. U.C.T. acknowledges support from the Deutsche Forschungsgemeinschaft (DFG) through a habilitation fellowship, DFG-Gz. Ta 177 / 2-1,2.

* Present address: Physics Department, Virginia Polytechnic Institute and State University, Blacksburg, VA 24061–0435, U.S.A.

[1] See, e.g., J.J. Binney, N.J. Dowrick, A.J. Fisher, and M.E.J. Newman, *The Theory of Critical Phenomena* (Clarendon Press, Oxford, 1993); J. Cardy, *Scaling and Renormalization in Statistical Physics* (Cambridge University Press, Cambridge, 1996).

[2] B. Widom, J. Chem. Phys. **43**, 3892 (1965); K.G. Wilson and J. Kogut, Phys. Rep. **12C**, 75 (1974).

[3] D.J. Amit, *Field Theory, the Renormalization Group, and Critical Phenomena* (World Scientific, Singapore, 1984); J. Zinn-Justin, *Quantum Field Theory and Critical Phenomena* (Clarendon Press, Oxford, 1993).

[4] A.M. Polyakov, Sov. Phys. JETP Lett. **12**, 381 (1970); A.A. Belavin, A.M. Polyakiv and A.B. Zamolodchikov, Nucl. Phys. B **241**, 333 (1984); D. Friedan, Z. Qui, and S. Shenker, Phys. Rev. Lett. **52**, 1575 (1984); J.L. Cardy, in *Phase Transitions and Critical Phenomena*, Vol. 11, eds. C. Domb and J.L. Lebowitz (Academic Press, New York, 1987).

[5] B. Schmittmann and R.K.P. Zia, in *Phase Transitions and Critical Phenomena*,Vol. 17, eds. C. Domb and J.L. Lebowitz (Academic Press, New York, 1996).

[6] V. Privman, A.M.R. Cadilhe, and M.L. Glasser, J. Stat. Phys. **81**, 881 (1995); D. Balboni, P.-A. Rey, and M. Droz, Phys. Rev. E **52**, 6220 (1995).

[7] K. Kang and S. Redner, Phys. Rev. A **30**, 2833 (1984).

[8] M. Doi, J. Phys. A **9**, 1479 (1976); P. Grassberger and P. Scheunert, Fortschr. Phys. **28**, 547 (1980); L. Peliti, J. Phys. (Paris) **46**, 1469 (1984); B.P. Lee, J. Phys. A **27**, 2633 (1994).

[9] P. Grassberger, F. Krause, and T. van der Twer, J. Phys. A **17**, L105 (1984); H. Takayasu and A.Yu. Tretyakov, Phys. Rev. Lett. **68**, 3060 (1992); N. Menyhárd and G. Ódor, J. Phys. A **28**, 4505 (1995); K.E. Bassler and D.A. Browne, Phys. Rev. Lett. **77**, 4094 (1996); Phys. Rev. E **55**, 5225 (1997); H. Hinrichsen, Phys. Rev. E **55**, 219 (1997); J.L. Cardy and U.C. Täuber, Phys. Rev. Lett. **77**, 4780 (1996); J. Stat. Phys. **90**, 1 (1998).

[10] J. Krug and H. Spohn, in *Solids far from Equilibrium: Growth, Morphology and Defects*, ed. C. Godrèche (Cambridge University Press, Cambridge, 1990); A.L. Barabási and H.E. Stanley, *Fractal Concepts in Surface Growth* (Cambridge University Press, Cambridge, 1995); J. Krug, Adv. Phys. **46**, 139 (1997).
[11] M. Kardar, G. Parisi, and Y.-C. Zhang, Phys. Rev. Lett. **56**, 889 (1986); for reviews, see Ref. [10] and T. Halpin-Healy and Y.-C. Zhang, Phys. Rep. **254**, 215 (1995).
[12] *Percolation Structures and Processes*, eds. G. Deutscher, R. Zallen, and J. Adler, Ann. Isr. Phys. Soc. **5** (Adam Hilger, Bristol, 1983).
[13] P. Grassberger and K. Sundermeyer, Phys. Lett. **77B**, 220 (1978); J.L. Cardy and R.L. Sugar, J. Phys. A **13**, L423 (1980); H.K. Janssen, Z. Phys. B **42**, 151 (1981).
[14] P. Grassberger, Math. Biosci. **63**, 157 (1982); J.L. Cardy, J. Phys. A **16**, L709 (1982); H.K. Janssen, Z. Phys. B **58**, 311 (1985).
[15] H.K. Janssen, Phys. Rev. Lett. **78**, 2890 (1997).
[16] U.C. Täuber, M.J. Howard, and H. Hinrichsen, Phys. Rev. Lett. **80**, 2165 (1998); the one-loop results were also independently derived by Y.Y. Goldschmidt (unpublished).
[17] J.L. Cardy, in *Proceedings of mathematical beauty of physics*, ed. J.-B. Zuber, Adv. Ser. in Math. Phys., Vol. 24, 113 (1997).
[18] B.P. Lee and J.L. Cardy, J. Stat. Phys. **80**, 971 (1995); M.J. Howard and J.L. Cardy, J. Phys. A **28**, 3599 (1995); P.-A. Rey and M. Droz, J. Phys. A **30**, 1101 (1997).
[19] We thank an anonymous referee for pointing this out to us.
[20] A.A. Migdal, A.M. Polyakov, and K.A. Ter-Martirosyan, Phys. Lett. B **48**, 239 (1974); H.D.I. Abarbanel and J.B. Bronzan, Phys. Rev. D **9**, 2397 (1974); J.B. Bronzan and J.W. Dash, Phys. Rev. D **10**, 4208 (1974).
[21] F. van Wijland, K. Oerding, and H.J. Hilhorst, Physica A **251**, 179 (1998).
[22] H.K. Janssen, cond-mat/9901188 (1999).
[23] The calculation presented in [16] is in error on this point. The correct exponent is given in Y.Y. Goldschmidt, Phys. Rev. Lett. **81**, 2178 (1998), and in the present work; see also U.C. Täuber, M.J. Howard, and H. Hinrichsen, Phys. Rev. Lett. **81**, 2179 (1998).
[24] H.D.I. Abarbanel, J.B. Bronzan, A. Schwimmer and R.L. Sugar, Phys. Rev. D**14**, 632 (1976).
[25] A. Aharony, J. Imry, and S-K. Ma, Phys. Rev. Lett. **37**, 1364 (1976).
[26] D.J. Amit and Y.Y. Goldschmidt, Ann. Phys. (NY) **114**, 356 (1978).
[27] For a review, see W. Kinzel, in Ref. [12], p. 425.
[28] E. Domany and W. Kinzel, Phys. Rev. Lett. **53**, 311 (1984); W. Kinzel, Z. Phys. B **58**, 229 (1985).
[29] K. B. Lauritsen, K. Sneppen, M. Markosová, and M. H. Jensen, Physica A **247**, 1 (1997).
[30] P. Grassberger, J. Phys. A **22**, 3673 (1989); P. Grassberger and Y.-C. Zhang, Physica A **224**, 169 (1996).
[31] P. Grassberger and A. de la Torre, Ann. Phys. (N.Y.) **122**, 373 (1979).
[32] H.K. Janssen, B. Schaub, and B. Schmittmann, Z. Phys. B **73**, 539 (1989); H.W. Diehl and U. Ritschel, J. Stat. Phys. **73**, 1 (1993).
[33] J.F.F. Mendes, R. Dickman, M. Henkel, and M.C. Marques, J. Phys. A **27**, 3019 (1994).
[34] D. Richardson, Proc. Camb. Phil. Soc. **74**, 515 (1973); N. Goldenfeld, J. Phys. A **17**, 2807 (1984); J.M. Kim and J.M. Kosterlitz, Phys. Rev. Lett. **62**, 2289 (1989); J. Kertész and D.E. Wolf, Phys. Rev. Lett. **62**, 2571 (1989); C. Lehner, N. Rajewsky, D.E. Wolf, and J. Kertész, Physica A **164**, 81 (1990); A. Toom, J. Stat. Phys. **74**, 91 (1994); J. Stat. Phys. **74**, 111 (1994).
[35] U. Alon, M.R. Evans, H. Hinrichsen, and D. Mukamel, Phys. Rev. Lett. **76**, 2746 (1996); Phys. Rev. E **57**, 4997 (1998).
[36] J.M. López and H.J. Jensen, Phys. Rev. Lett. **81**, 1734 (1998).
[37] T. Sams *et al.*, Phys. Rev. Lett. **79**, 313 (1997).
[38] M.J. Howard and U.C. Täuber, J. Phys. A **30**, 7721 (1997).